



Università degli Studi di Salerno

Dipartimento di Ingegneria Elettronica ed Ingegneria Informatica

Dottorato di Ricerca in Ingegneria dell'Informazione
XI Ciclo – Nuova Serie

TESI DI DOTTORATO

**Carbon nanotube based
networks,
bio-nano-composites
and sensors.**

CANDIDATO: **RAFFAELE DI GIACOMO**

TUTOR: **PROF. HEINRICH C. NEIZERT**

COORDINATORE: **PROF. ANGELO MARCELLI**

Anno Accademico 2011 – 2012

Carbon nanotube based networks, bio-nano-composites and sensors.

Introduction

I.1 Electrical conductivity of carbon nanotubes networks

I.2 The influence of the external contacts on CNTs networks and devices

I.3 CNT based field effect transistors

I.3.1 CNT-based FET.

I.3.2 CNN-based FET.

I.4 Novel CNT Bio-nano-composites and their application

Chapter 1

Substrates for pure CNT networks and microscopy investigation of CNT interconnections

1.1 Substrate preparation and characterization

1.1.1 Introduction

1.1.2 Experimental

1.1.3 Breakdown formation

1.1.4 Photo detector characterization

1.2 Microscopy of carbon nanotubes

1.2.1 Preparation of the sample

1.2.2 Investigation of the MWCNTs interconnection geometry

1.3 Conclusions

Chapter 2

Carbon Nanotube Networks

2.1 Technology for pure CNT networks production

- 2.1.1 Preparation of the solutions
- 2.1.2 Aluminum gap and substrate
- 2.1.3 Casting di-electrophoresis
- 2.1.4 Network Morphology
- 2.1.5 Characterization equipment

2.2 Electrical characterization

- 2.2.1 Stabilization and noise behavior
- 2.2.2 Stable characteristics and temperature behavior

2.3 Conclusions

Chapter 3

Bio-nano-technology and tissue engineering for electronic and mechanical purposes

3.1 *Candida albicans*/MWCNTs: a stable conductive bio- nano-composite.

3.1.1 Sample production and morphology

3.1.2 Thermo-electrical characterization

3.2 Cyborg tissues constructed with whole cells and carbon nanotubes: bio-materials for engineering applications

3.2.1 Material production

3.2.2 Material morphology

3.2.3 Electrical characterization

3.2.4 Mechanical characterization

3.2.5 Optical characterization: a transparent and conductive film

3.3 Conclusions

Introduction

In this thesis different techniques are used to produce sensors and bio materials in which carbon nanotubes (CNTs) play the active role and are the main molecules used to drive current and obtain mechanical stability. The work is organized as follows:

Chapter 1 describes the basics of the technology used to produce pure CNT sensors without any matrix. The Silicon dioxide films onto which the CNTs are deposited are characterized in order to determine their thickness and eventual defects. After deposition the utilized CNTs and their interconnection geometry are visualized by a detailed microscopy investigation.

Chapter 2 is focused on the stabilization of the electrical characteristics of CNTs networks in an aluminum contact micro-gap. It also reports the utilization of such structures as temperature sensing elements.

In Chapter 3 novel bio-nano-composite materials and their use as temperature sensing elements are described. Furthermore a general procedure to obtain cyborg tissue useful for mechanical, electrical and optical applications is also reported.

As one of the major skills while dealing wet deposition of CNTs is the preparation of the solution. Each chapter has a detailed description of the used techniques and solvents/surfactants.

This introduction starts with a brief discussion regarding the electrical conductivity of CNTs and on the factors that affect this parameter. Then in order to explore the reasons of the choice of CNTs, examples of field effect transistor based on carbon nanotubes are given as one of the most promising application of such nanomaterials as new electronic components. Successively in this introduction the state of the art of CNT based temperature sensors is presented together with the new idea of using whole biological cells as matrices for material production.

In the last part of this introduction we focus on the production of bio-materials with different cell types and for different applications and thus introduce the new concept of cyborg tissues.

I.1 Electrical conductivity of carbon nanotubes networks

The electrical conductivity of a CNT network without matrix alone or inside a matrix as composite material can be described by the percolation theory [1,2] and depends on a number of factors. It is strongly dependent on the CNT concentration such that for a given composite it can vary by more than 10 orders of magnitude in dependence of such parameter [3]. In general a so called percolation threshold is observed as the minimum CNT concentration from which the conductivity starts to increase strongly.

An accurate model, however, has to take into account also a large variety of other parameters, as for example the CNTs aspect ratio, the conducting type (semiconductor or metallic) of the nanotubes and the type of interconnection between the single nanotubes [4]. In the case of linear low density polyethylene (LLPE/CNT) composite materials, modifications of the sample conductivity during high temperature thermal cycling have been mainly attributed to the improvement of the CNT-CNT interconnections [5].

The effect of the nanotube/nanotube contact resistance on the electrical conductivity of CNTs based nano-composites has been studied using different approaches. As an example a rectangular potential barrier in the insulating material between two nanotubes has been assumed for the calculation of the tunneling resistance of two crossing multi walled CNTs (MWCNTs) [6]. A detailed analysis of the electrical characteristics of CNT composites also making use of low frequency noise spectroscopy, gives strong indications that the resistance of the CNT-CNT interconnection is dominating the overall resistance of carbon nanotube networks (CNNs) rather than the resistivity of the nanotubes themselves. In particular the $1/f$ noise in carbon nanotube random network films has been found to be dominated by the percolation process [7].

Low-frequency noise spectroscopy has been applied also to the analysis of the interconnection properties of high density polyethylene/MWCNT composites and fluctuation induce tunneling (FIT) has been found to be the dominating mechanism [8, 9]. The same holds in the case of Epoxy/MWCNT composites [10]. The latter

system has a very low percolation threshold and is furthermore very attractive for electrical applications as for example as an electrical heating element and as a temperature sensor with good stability up to 200°C [11] and as microwave absorber [12].

In polymer/CNT composites due to the presence of the matrix, it is in general difficult to obtain a clear microscopy image of the incorporated Carbon Nanotube Network (CNN). This holds also in the case of high density pure CNT networks alone. Therefore, in order to get a better insight into the CNT interconnection geometry, it is preferable to investigate also low-density CNT networks without matrix.

For example the geometry of a single junction between two MWCNTs has been explored using SEM imaging and it has been found that in some cases a simple proximity of the MWCNTs is present. In this case the electrical characteristic exhibited rectifying behavior which had been explained by the formation of a Schottky barrier junction [13]. With respect to this aspects in this thesis in *Chapter 1* the microscopy analysis of MWCNTs networks containing few nanotubes deposited by di-electrophoresis is reported. The application of various microscopy techniques, namely, scanning electron microscopy (SEM), atomic force microscopy (AFM) and focused ion beam (FIB) microscopy has been used in order to investigate the interconnection geometry of single junctions between MWCNTs.

I.2 The influence of the external contacts on CNTs networks and devices

Contact material and geometry are crucial for the performance of CNT based devices [14]. Most metal-CNT junctions behave more like Schottky barriers rather than purely ohmic contacts [15]. The modulation of CNT field effect transistors for example is believed to be rather due to the modulation of the electronic barrier at the semiconductive CNT–metal contact interface by the applied gate voltage than to a modulation of the channel conductance itself [16]. Contact interface problems are often thought to be the dominating source of electrical noise.

This has been reported for example in CNT transistors with Ti/Au as contact material where a large random telegraph signal has been observed and attributed to a defect located in the drain side of the Schottky barrier [17]. In the case of an aluminum/CNT contact also the presence of a thin aluminum oxide film, which may contain a high defect density [18], has to be considered.

Random telegraph noise has been explained as a random charging and discharging of defects in levels energetically close to the CNT Fermi level [19, 20]. Electrical bistability observed in the current-voltage characteristics of CNT/metal contacts is also often exploited for electrical switching devices. An example of such a bistable device is the deposition of Ag-tetracyanoquinodimethane (AgTCNQ) embedded between two crossed carbon nanotubes as electrode contacts [21].

In devices where no bistability has been observed and metal contacts to CNT devices show a good ohmic behavior, in general a $1/f$ noise component dominates the low-frequency noise spectrum [22], [23]. This noise component has been largely attributed to the nanotube network itself rather than to the external contacts.

One of the most used techniques in literature used to produce pure nanotube networks is the di-electrophoresis process. The construction of carbon nanotube field effect transistors (CNT-FETs) for example, can be accomplished with proper tuning of the di-electrophoresis parameters. Even the formation of CNT networks with predominately semiconductive characteristics has been achieved [24]. Di-electrophoresis has also been shown to enable the reproducible assembly of a single bundle of single-walled carbon nanotubes [25].

For the successful deposition, the type of surfactant that enables a proper solution of the nanotubes in the solvent is very important. In the case of sodium-dodecyl-sulfate (SDS) the surfactant molecules form an ionic layer encapsulating the nanotubes by surface adsorption and the nanotube-micella complex formed has a greater polarization than that of the SWNTs alone [26].

In *Chapter 2* the di-electrophoresis has been described for the deposition of a pure MWCNTs network inside an aluminum gap. The samples after an initial instability acquire an ohmic behavior and the temperature dependence of the electrical conductivity could be well described by the fluctuation induced tunneling model.

I.3 CNT based field effect transistors

One of the most promising field in which CNTs will play a major role in the future is the realization of new types of transistors. The first purely carbon based transistors were realized with diamonds, (see for example [27]). Then in the late nineties CNT based transistors have been realized for the first time [28] and became mature within few years. An important division among CNT transistors can be made between single nanotube devices (see Fig.I.1a), in general realized with single walled carbon nanotube (SWCNT) or in some cases also with multi-walled carbon-nanotube (MWCNT), and those made of carbon nanotube networks (CNNs) (see Fig.I.1b). Even if the history of graphene based FETs is very recent (2004) [29], they already outperform the more consolidated CNT based transistors regarding some specific performances. I will give a short historical review and a comparison of the most promising applications of these different types of all-carbon based field effect transistors (see Fig.I.2). The main reason for which carbon based structures are very attractive as active material for FETs is because of the high carriers mobilities that have been reported for CNTs and graphene. In the case of carbon nanotubes a field-effect mobility of $79000 \text{ cm}^2/\text{Vs}$ and an estimate intrinsic mobility higher than $100000 \text{ cm}^2/\text{Vs}$ has been reported [30].

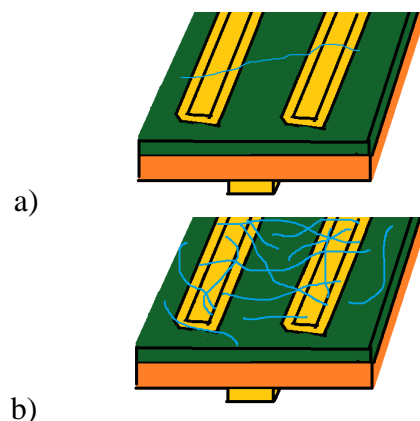


Fig. I.1. Schematical drawing of a) single carbon-nanotube FET and b) a carbon-nanotube network FET, in bottom-gate configuration

Even higher charge carrier mobilities ($>200000 \text{ cm}^2/\text{Vs}$) have been reported by using a device structure, where a single layer of graphene is suspended above a Si/SiO₂ system as gate electrode and isolator material respectively [31].

Last but not least, also CNNs based carbon-nanotube thin-film transistors (TFTs), deposited on a polymeric substrate, have been reported with rather high mobilities [32] as compared to the alternative TFT technologies (organic material or amorphous silicon).

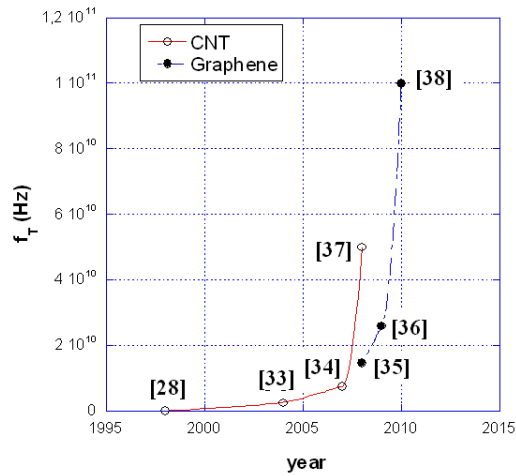


Fig. I.2. Historical development of the maximum frequency (f_T) of carbon nanotube and graphene based transistors. The related article reference numbers have been indicated.

I.3.1 CNT-based FET

In 2008 Chaste et al. reported on microwave frequency operation of a top-gated single carbon nanotube transistor. They demonstrated the operation of a SWNT-FET up to a frequency of 1.6 GHz with rather high transconductance values and observed, that high sensitivity is preserved and that gate capacitance scales with gate lengths down to 300 nm. Transit frequencies as high as 50 GHz have been extrapolated [37].

I.3.2 CNN-based FET

Vaillancourt et al. reported in 2008 the realization of a flexible carbon nanotube thin-film transistor, fabricated solely by ink-jet printing technology. The TFT was top gate configured. As active channel material they used an ultrapure, high-density (>1000 CNTs/ μm^2) CNT thin film, as gate isolator an ion-gel dielectric layer and as top gate electrode a poly(3,4-ethylenedioxythiophene) organic layer. This CNT-TFT exhibits a high operating frequency of over 5 GHz and an on-off ratio exceeding 100 [39].

It has been just over 9 years since graphene based electronic devices were first reported, and since then a remarkable progress regarding its application for high frequency transistors has been achieved [40]. However, carbon nanotube based transistors, have also reached a technologically relevant status and also in their case high speed operation has been demonstrated. CNN based transistors, on the other hand, can be easily deposited by low-cost printing techniques on arbitrary substrates and are rivalling organic and amorphous silicon TFTs in a wide range of applications.

I.4 Novel CNT Bio-nano-composites and their application

As mentioned before, CNTs are known to improve the electrical conductivity when used as fillers in composite materials [41] and combined with different polymers matrices [42-44] they can be used as temperature sensors. CNTs are also known to interact with cells without causing significant decrease of viability [45] and when functionalized they can cross cellular barriers [46].

CNTs alone, e.g. in a long suspended array, act as temperature sensors with a high sensitivity [47]. Addition of a matrix to CNTs generally results in a better long-term stability of the sensing element, compared to pure CNT bundles or sheets.

It has been shown that polymer matrix composites such as epoxy/MWCNTs can be used as temperature sensor in a wide range of

temperatures with an excellent stability and a linear temperature-resistance characteristics [42].

Cellulose, a structural component of the plant cell wall of several algae and oomycetes, has also been used to form CNTs/cellulose conductive composite materials through the formation of a CNT network on the cellulose fibers [48]. However, temperature analyses were not performed on this material though it exhibited good characteristics regarding its application as electromagnetic shielding material [48]. In other experiments MWCNTs were incorporated by electro-spinning in cellulose fibers, resulting in an improvement of the mechanical properties [49].

In this thesis (see **Chapter 3**) we used growing yeast cells of *C. albicans* as matrix for MWCNTs. Previously, studies on the toxicity of MWCNTs have shown that incubation of the yeast *Saccharomyces cerevisiae* in the presence of MWCNTs had no effect on growth and on cell viability of this organism [50].

These authors tracked the distribution of fluorescein isothiocyanate (FITC) functionalized MWCNTs inside the yeast cells by fluorescence microscopy. Moreover, it was shown by confocal microscopy, that MWCNT-FITC had been internalized inside the yeasts [51].

Functionalized CNTs, for their ability to penetrate inside the cells, have been used to deliver peptides, proteins and drugs. In addition, functionalized CNTs do not elicit an immune response when injected into an animal [51]. MWCNTs have been also used to deliver the gene coding for the Green Fluorescence Protein into mammalian cells with little or no cytotoxicity [52].

The mechanism by which CNTs enter the cells remains poorly understood. However, experiments using 3-D electron tomography techniques have shown that functionalized MWCNTs were internalized individually in human lung epithelial cells (A549), and primary macrophages cells via membrane wrapping or by direct membrane translocation [53].

The aim of the work, described in **Chapter 3** of this thesis is to develop, using growing cells, a bio-structured nano-composite for electrical applications. It has been reported that the bacterium *Pseudomonas aeruginosa* immobilized MWCNTs and that the

resulting structure could be used for bio absorption of heavy metal ions [54]. However, the mixture was obtained using dead bacteria.

The MWCNTs/bacteria ratio was very high and the dried cells were fixed in a MWCNT based “bucky paper” as shown in SEM images [54]. Though this was a good procedure in order to obtain a paste, it is different from the experiments in this thesis in which a *in vivo* self-structuring of an artificial tissue has been observed.

Differently from mixing two powders, in **Chapter 3** it is reported, how MWCNTs were utilized to connect cells.

The produced bio-nano-composite exhibits a linear thermo-electric behavior in the range from 25° to 100°C similar to pure nanotube networks produced with the same type of MWCNTs utilizing the same solvent [55].

If we look more generally for tissues, biological components from different sources (e.g. collagen) have been used to obtain nano-structured materials that are employed as synthetic scaffolds into which biological tissues have been applied [56-60]. Bio-composite materials for mechanical [61] or electrical [62] applications have also been produced.

Cyborg tissue is an open and promising field since development of synthetic biomaterials will effect greatly the production of new electronics and artificial materials [56]. Scaffolds that support cell growth and simultaneously monitor cell activities have been described [56].

Biodegradable three-dimensional (3D) structures that serve as short-term supports for cells and new tissue growth have been also formed with hydrogel [57] using inert synthetic molecules such as poly(ethylene glycol) [59]. Synthetic gels mediate the delivery of trophic factors for neural cell repair [58].

An artificial heterocellular 3D architecture has been used also to monitor the molecular behavior of cancer cells [60].

In all these cases, however, the cells applied into the scaffolds could naturally form tissues: so far no unicellular organisms or single cell lineages have been employed for tissue engineering and a procedure to generate cyborg tissue materials composed of whole cells and carbon nanotubes for engineering applications has not been reported yet.

In **Chapter 3** of this thesis a procedure is described, that allows to obtain novel artificial materials using, for example, either fungal or

isolated tobacco cells in combination with different concentrations of carbon nanotubes.

Chapter 1

Substrates for pure CNT networks and microscopy investigation of CNT interconnections

In this chapter the technology used to obtain pure CNTs networks is described and the resulting structures are characterized. A technique to characterize the silicon dioxide defects, formed during electrical breakdown of the isolating layer on the substrate and its use to produce photosensitive devices is reported. Preliminary methods to produce aluminium contacts, CNTs solution, and to deposit and form CNTs networks are also reported here. This aspects will be analysed more in detail in the following *Chapter 2*. The present chapter is furthermore focused on a detailed microscopy analysis of the CNTs used and of their topology and connections inside the networks.

1.1 Substrate preparation and characterization

To obtain pure CNNs and use them as sensors the insertion of an insulating layer on top of the substrate can be useful. Here SiO₂ represented the best choice for three main reasons: 1) it is relatively easy to produce, when Silicon is used as a substrate 2) CNTs normally exhibit a very strong adhesion to SiO₂ layers 3) it is very flat. However also a thermally grown SiO₂ layer can contain impurities that strongly affect its insulting properties. In this section a method to characterize this parameter in a novel manner is reported. Using this technique an interesting procedure to generate photosensitive devices on a Si/SiO₂ substrate, without the need of high temperature processes, has been found.

1.1.1 Introduction

Monitoring the current with and without illumination during the application of successively increasing voltages in a MOS structure

with impurity containing oxide layer, it was observed in-situ the formation of a photosensitive device.

For some applications it is interesting to make electronic devices, based on a silicon substrate without the application of temperatures exceeding 200°C after the deposition of a silicon dioxide isolation or passivation layer. This excludes the possibility to use either the classical method of dopant diffusion at elevated temperatures and also ion implantation for the emitter formation, because the latter technique requires a high temperature annealing step after implantation. One possibility is the deposition of a hetero-diode by the deposition of a non-crystalline silicon material on top of the crystalline silicon substrate.

A device of interest is a simple photodiode, that may in particular serve as a test structure for the silicon surface quality. Silicon photodiodes with a hetero-emitter are for example based on the deposition of a transparent conductive oxide (TCO) such as ITO [63] or on the deposition of amorphous silicon on top of the crystalline silicon substrate [64]. It should be mentioned that the latter device is one of the most efficient types of silicon based solar cells [65]. Recently it has been demonstrated that such a type of hetero-photodiode can also be achieved simply by spin-coating of an organic nanocomposite thin film on top of the crystalline silicon substrate [66]. Other techniques for the realization of photodiodes are involving a modification of the top silicon dioxide passivation layer. In particular it has been shown, that the formation of nanotracks by proton irradiation of SiO₂ covered Silicon can be used for the formation of electronic devices [67].

In the present paragraph it is presented a method for the reproducible fabrication of photodiodes using the local breakdown of an MOS capacitor with aluminum top metallization and an impurity containing oxide, that has been thermally grown on top of a crystalline silicon substrate.

1.1.2 Experimental

MOS structures were prepared oxidizing 575 μm thick, <100> oriented, boron doped p-type CZ-Silicon wafers with a resistivity of nominally 2-3 Ωcm. The oxidation process was performed at 1000°C

for 120min and subsequently at 1185°C for 10min in a furnace not dedicated to this processes only with a high probability of impurity incorporation. The resulting oxide thickness was measured to be 109nm. Non transparent 100nm thick aluminum pads with an rectangular geometry (see Fig.1.1) and an area of 6mm² were produced by a lift off process. The back contacted wafer was placed on a copper plate and the top contact pads were contacted by a probing needle.

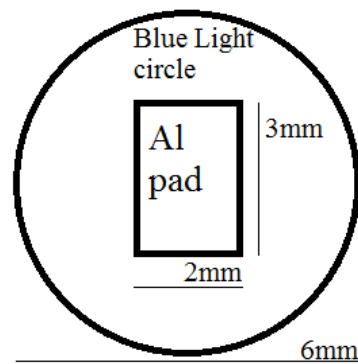


Fig 1.1. Blue light spot and geometry of the top aluminum pad.

The current-voltage characteristics of the MOS capacitor has been measured with and without illumination at room temperature using a Keithley 2400 source measurement unit. Light intensity dependent current-voltage characteristics were performed under two different illumination conditions: In the first case a white light LED lamp with a broad emission spectrum between 425nm and 770nm (see Fig.1.2) has been used for illumination and the optical power has been varied using different distances (between 2cm and 30cm) between the device under test and the lamp. In this case the silicon substrate with an area of 1cm² containing 6 different MOS structures has been illuminated completely. The average light power has been determined using a calibrated Hamamatsu S2386-18K Silicon photodiode.

In a second illumination configuration, a blue LED with an emission wavelength centered at 470nm has been placed at a short distance from the sample with an illuminated area of only 28mm² (see Fig.1.1). The light intensity of the LED was changed by varying the

LED current and measured using the calibrated Silicon photodiode. The emission spectrum of the blue LED is shown in Fig.1.3.

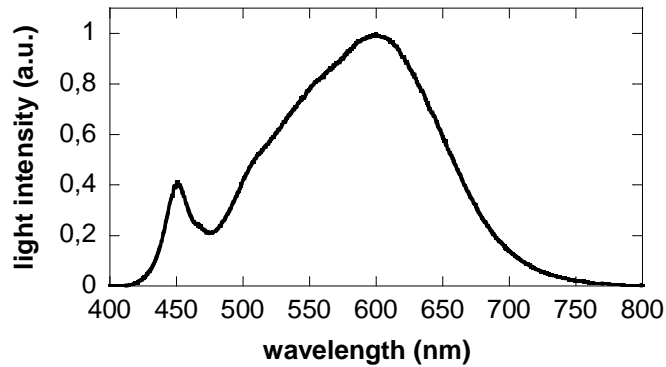


Fig 1.2. Emission spectrum of the white LED light source.

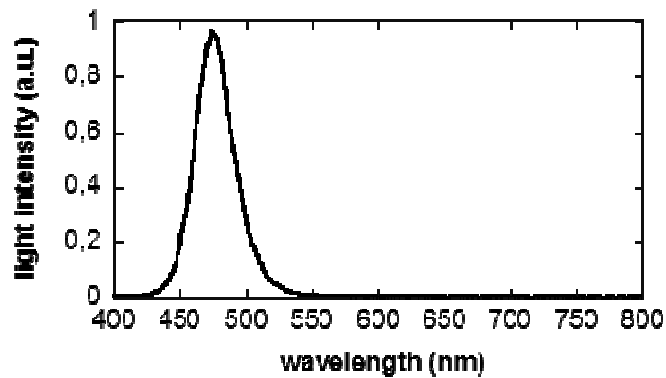


Fig 1.3. Emission spectrum of blue LED light source.

1.1.3. Breakdown formation

After a complete device characterization before degradation in a restricted voltage range of $\pm 15\text{V}$, a first increasing and then decreasing voltage ramp was applied up to 80V in steps of 1V . The whole measurement cycle, shown in Fig.1.4, lasted only 30s. Up to a voltage of about 50V , a relatively low dark current of about 1nA slightly dependent on the applied voltage was observed. It should,

however, be noted that the resulting conductivity of the oxide is way above the value for a good thermal oxide. This can be attributed to the effect of incorporated impurities, as already mentioned in the experimental section.

In the voltage range between 50V and 70V it can be seen a rather noisy current-voltage characteristics due to the local breakdown formation and self-healing effects. At 60V, the formation of a first current plateau of about 100nA and then around 70V a second plateau of about 1 μ A are observed. Finally at 80V, complete breakdown is observed, resulting in a sudden strong increase of the current to a value of almost 1mA. During the subsequent measurements for decreasing applied voltages the current remained high with values above 10 μ A down to an applied voltage of 2V.

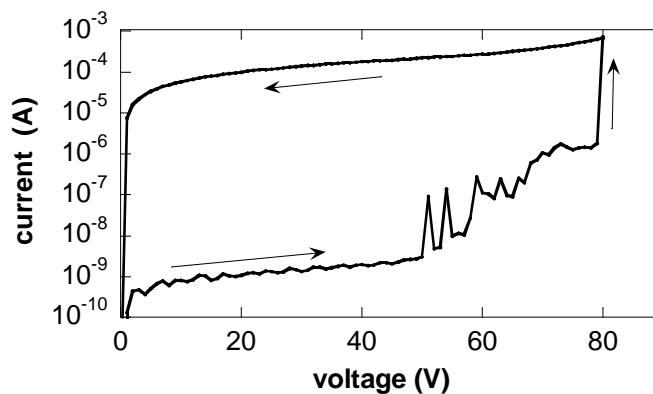


Fig. 1.4. Dark current monitoring during an upward and downward voltage sweep up to a maximum voltage of 80V.

In a subsequent experiment the formation of the photoconductivity by additionally illuminating the device with a blue LED light was monitored. The measurement is shown in Fig.1.5. It can be seen that below the first breakdown at 40V the device is not photosensitive. A very similar development of the dark current with increasing voltages as in the earlier reported case (Fig.1.4) is observed with the second plateau reached at about 55V. Between 50V and 60V the ratio between photo- and dark-current increases linearly to a value of about 80 and remains stable until the second breakdown occurs slightly below 90V.

Comparing the photo- and dark-current during the decreasing voltage sweep from 90V down to 0V (Fig.1.5), the highest ratio between photo- and dark-current is found for applied voltages between 2V and 10V. It has been shown in literature, that the monitoring of dark- and light current-voltage characteristics during degradation of vertical cavity surface emitting and edge emitting lasers due to electrostatic discharge pulse application gives valuable insights into the device degradation mechanisms [68,69]. Furthermore also the defect induced formation of high photo-gain in pin-photodiodes has been reported [70].

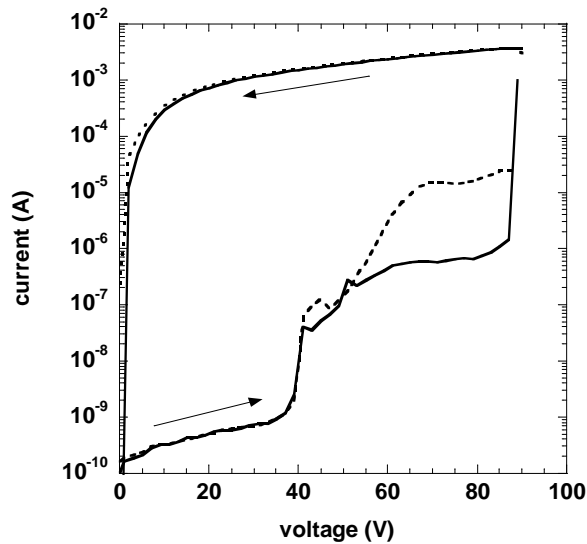


Fig 1.5. Dark (Solid line) and blue LED illuminated (dashed line) current monitoring during an upward and downward voltage sweep up to a maximum voltage of 80V.

1.1.4 Photo detector characterization

In Fig.1.6 the current-voltage characteristics of the degraded MOS device, whose formation has been monitored before (see Fig.1.4) is shown with and without illumination with the white light source for different light intensities. The light intensities have been referred to a

P_0 value, corresponding to an optical power density of about $25\text{mW}/\text{cm}^2$.

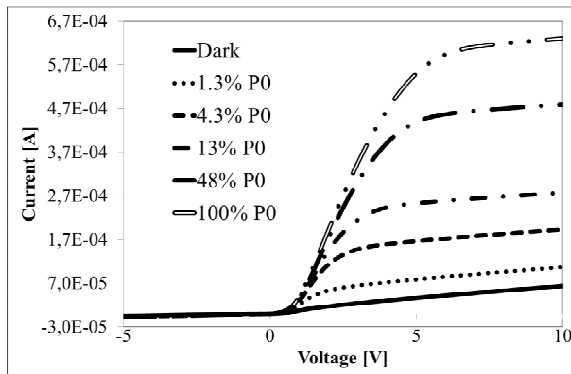


Fig. 1.6. Current-voltage characteristic measured after degradation with and without illumination with white LED light with different intensities.

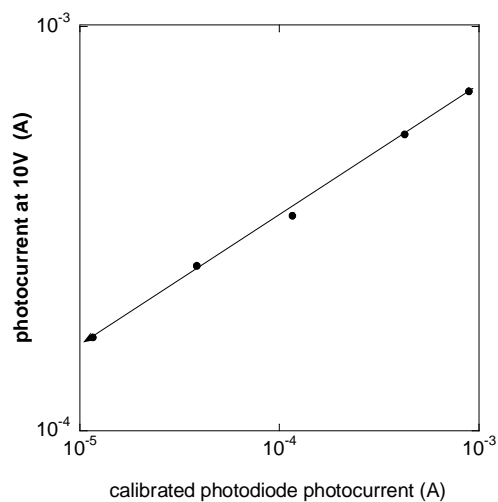


Fig. 1.7. Dependence of the photocurrent generated in the MOS structure for an applied voltage of +10V to the top contact as a function of the light intensity, as measured by the photocurrent generated under short circuit condition in a calibrated photodiode with identical illumination conditions.

The photo- to dark-current ratio is strongly increasing between 1V and 5V and saturating between 5V and 10V. When plotting the photocurrent values at an applied voltage of 10V as a function of the calibrated reference photodiode current a power-law behavior is found.

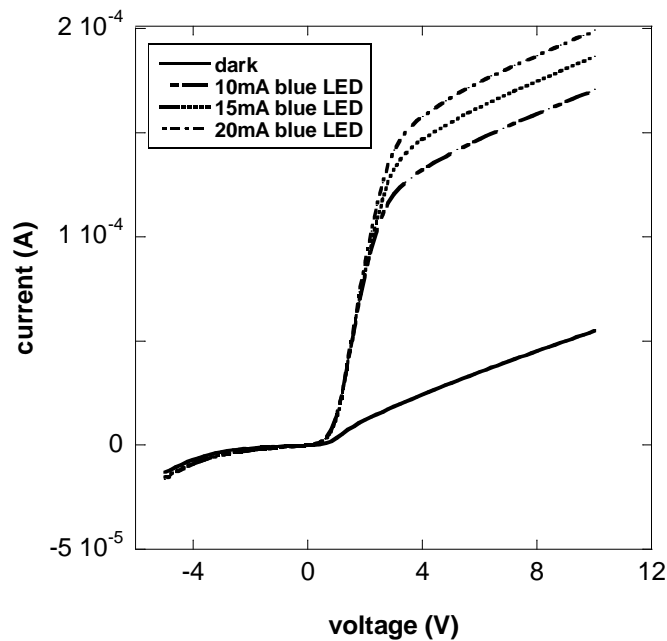


Fig. 1.8. Photo generated current in the sample device as a function of the incident optical power.

The behavior of the photoresponse of the structure to blue light with 470nm wavelength is shown in Fig.1.8. There is a strong increase of the photoconductivity with increasing voltage between 0.5V and 2V, followed by a region, where the photocurrent value is strongly dependent on the incident light power.

Again the dark and light current-voltage characteristics in this latter voltage range are parallel. This suggests the interpretation of the results by the formation of a local p-n junction and a parallel shunt resistance. The absence of primary photocurrent at 0V applied bias may be due to the additional existence of a blocking contact.

It should be mentioned, that this devices are by no means optimized as photoreceivers, because the top metallization is not transparent for the light.

This means that lateral diffusion of the photocarriers, generated in the silicon substrate, to the electrical contact region substrate has to be accounted for.

1.2 Microscopy of carbon nanotubes

In recent years a very large amount of data has been collected regarding devices formed by MWCNTs in polymer matrix as well as single nanotubes.

In contrast very little investigations exist over nanotubes networks constituted by a small number of MWCNTs. In this section a detailed investigation of the long time stability, adhesion to the surface and topological structure of the interconnections between MWCNTs has been done. Three different microscopy techniques, Focused Ion Beam (FIB),

Scanning Electron Microscope (SEM), and Atomic Force Microscope (AFM), were used in order to investigate the interconnection of MWCNTs deposited by electrophoresis on a thermally oxidized silicon wafer with aluminum microgap structure. SEM, AFM and FIB imaging revealed an interesting interconnection morphology between the drop casted MWCNTs.

In particular it was found that in some cases the MWCNTs were connected to each other in a twisted geometr. Furthermore a good stability of the sample has been observed proving a strong adhesion of the tubes to the SiO₂ surface.

1.2.1 Preparation of the sample

Two aluminum contacts with a gap of 3 μ m (see Fig.1.9) were prepared using a lift off process on top of a thermally oxidized (100nm thick SiO₂ film) p-type silicon substrate with a conductivity of 20Ohmcm.

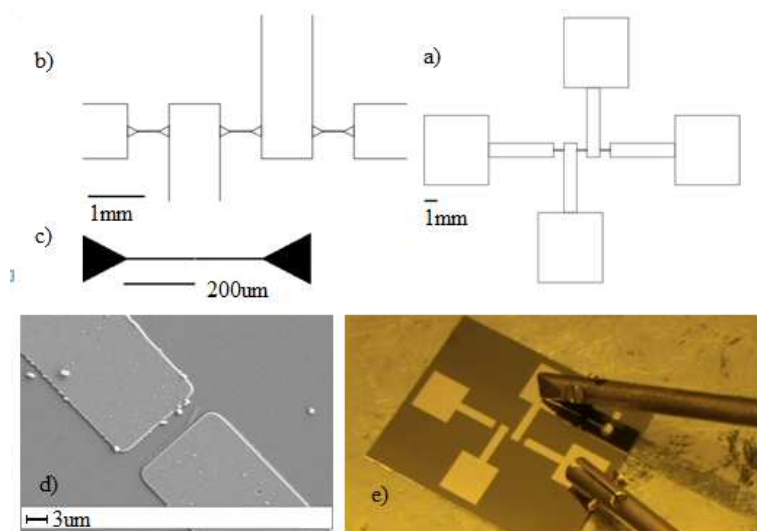


Fig. 1.9 Lateral structure of the used substrates with a microgap, realized by Aluminum evaporation on top of a p-type silicon substrate covered by a 100nm thick SiO_2 . a) Mask design, three gaps inside three stripes are connected to 25mm^2 large contact pads b) zoom into the stripe regions: triangles at the stripe ends were designed c) right end stripe with a $3\mu\text{m}$ gap d) SEM picture of the micro gap region e) photo of a finished substrate contacted by contact needles before electrophoresis.

A small quantity of MWCNTs has been added in highly deionized water with 1% sodium dodecyl sulfate (SDS). The solution has been sonicated for 20min at room temperature. A small drop was taken from the supernatant part of the solution in order to avoid cluster residues and deposited on top of oxidized silicon wafer substrate heated to a temperature of 50°C . During casting, electrophoresis was performed to drive MWCNTs into the gap by means of a sinusoidal electric field with a frequency of 15MHz and an amplitude of 10V, using a HP 33120A waveform generator.

The AFM Measurements were performed in Salerno University with an AFM of the following characteristics: Bruker dimension 3100, with controller Nanoscope V. Images were obtained in tapping acquisition mode with a tip with final reduction of 1-2nm and a scan rate 0.5 Hz. The SEM and FIB pictures were obtained by using a DUALBEAM

FIB, located at the TU Berlin. This FIB using a Ga⁺ ion beam for imaging, is also equipped with a SEM. Since MWCNTs can be assumed to exhibit metallic behaviour the images were obtained without covering the sample with a conductive layer. The FIB imaging is due to the secondary electron emission. In our case the image shown was obtained with an incident ion beam with 30kV voltage and 4pA current.

1.2.2 Investigation of the MWCNTs interconnection geometry

During the MWCNTs solution preparation at the beginning of the sonication process the MWCNTs were massed in few macro clusters thus the water resulted transparent. At the end of the sonication process the water became darker because the MWCNTs were nano-dispersed. Electrophoresis revealed to be a mandatory procedure during casting of MWCNTs. As the substrate was heated to permit the water to evaporate, electrophoresis permitted to avoid the complete accumulation of the MWCNTs on the circular edge of the drop once the water was completely evaporated.

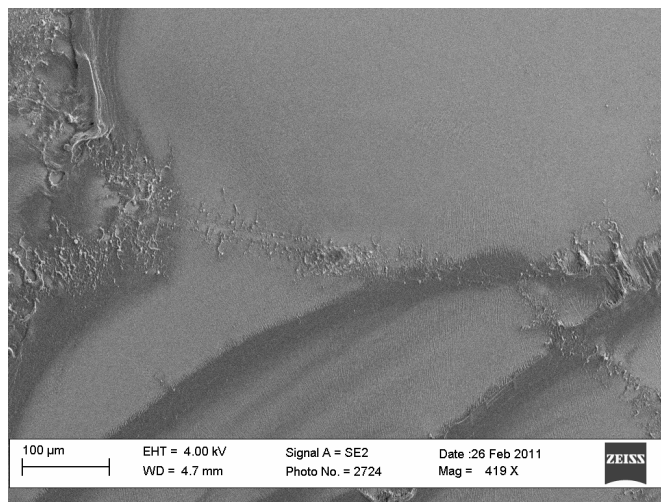


Fig. 1.10 SEM image of a microgap region with MWCNTs deposited by electrophoresis

With this procedure a very high concentration of tubes has been captured in the center of the microgap and it was observed a compaction of the material along the lines of the electric field as shown in Fig. 1. 10. Despite the small quantity of material deposited, a very high concentration of MWCNTs was found inside the gap. At this concentration it was impossible to determine the nature of the single interconnections between tubes. As a benefit of the electrophoresis the amount of material clustered into the gap and contact region was subtracted from the edge of the dried drop. In Fig. 1.11 an area along the drop edge is shown.

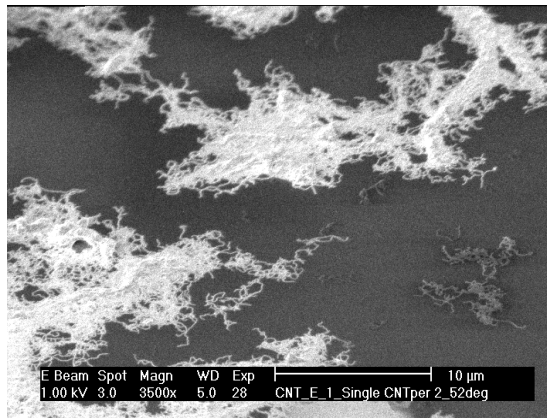


Fig. 1.11 SEM image of a MWCNT network found outside the microgap region. Angle of the sample 52°

It is possible to distinguish nanotubes and interconnections and in the upper left corner three single tubes connecting two bundles can be seen. Since the image was taken using an electron beam it is possible to see the voltage contrast effect for which darker tubes are to be considered electrically isolated while brighter tubes are connected to at least one of the grounded aluminium electrodes. Moving further away from the center of the drop passing the edge it can be observed a region where the concentration of tubes is sensibly lower and thus it is possible to identify single connections between tubes. In Fig. 4 three main tubes connected to each other twisting at their end are observed.

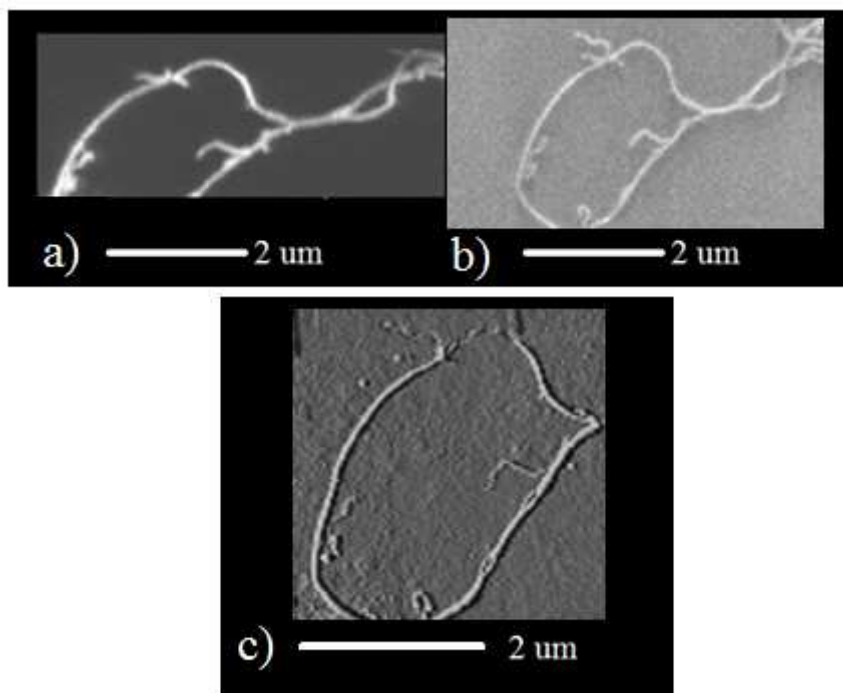


Fig. 1.12 FIB, SEM and AFM images of few interconnected MWCNTs forming a loop a) Ion Beam image (FIB). Voltage:30kV, Current:4pA, Working Distance: 16.5. Angle of the sample: 52° b) SEM image. Voltage: 3KV, Working Distance: 5. Angle of the sample: 0° c) AFM amplitude error image. (Acquisition mode: tapping, tip final reduction: 1-2nm, scale: 20mV, scan rate: 0.5 Hz)

The resulting cord is disposed in a circular shape. The geometry of one of the interconnections between MWCNTs is seen in more detail in Fig. 1.13 and Fig. 1.14.

This connection exists between two of the main tubes described before. The junction is clearly visible in the images taken with the sample plane tilted by 52° (see Fig. 1.12a and Fig. 1.13). When the sample plane is not tilted a third tube becomes visible (Fig. 1.12b,c and Fig. 1.14). Further observation permits to identify the nature of the connection between tubes.

Proceeding from left to right in Fig. 1.13 the first tube is winding over the successive one and terminating with a protruding part heading down right the image frame. This first tube seems to

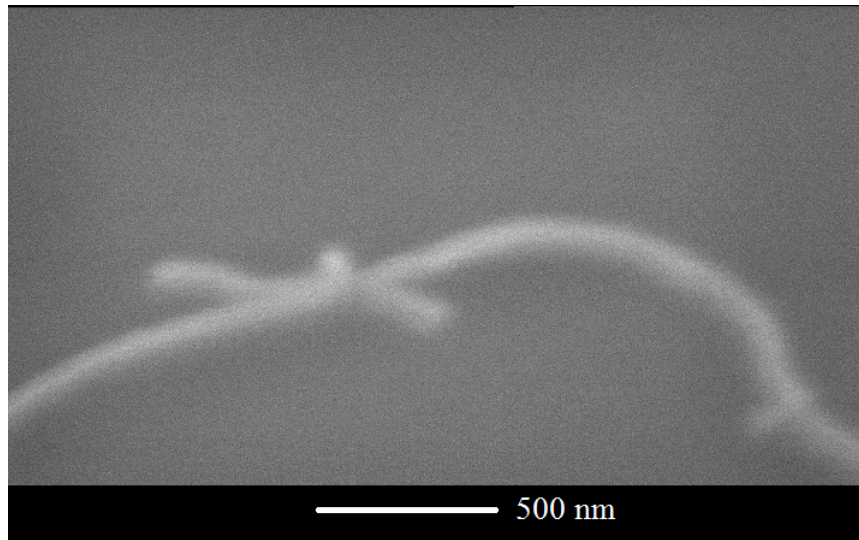


Fig.1.13 SEM image of the contact region between 2 single MWCNTs within the CNT loop shown above.
(Voltage: 3,5kV, Working Distance: 5, Angle of the sample: 52°)

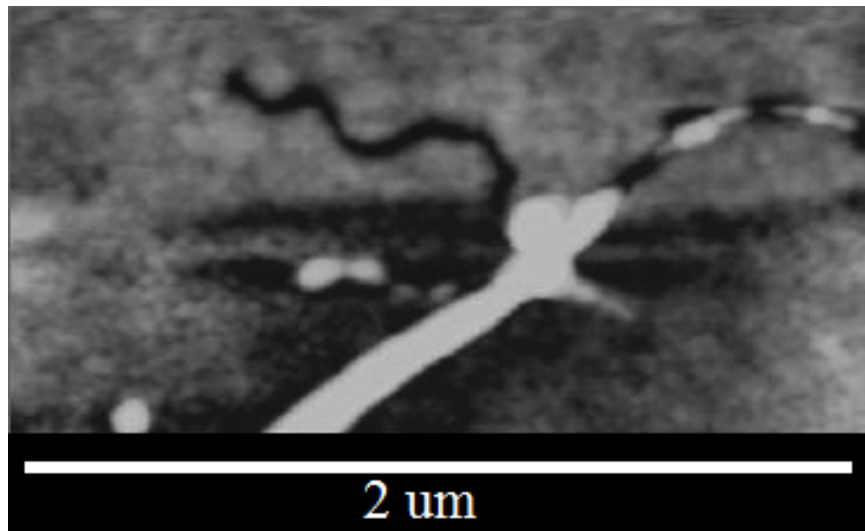


Fig. 1.14 AFM height image. Acquisition mode: tapping, Tip final reduction: 1-2nm, Scale: 15nm, Scan rate: 0.5 Hz

elevate from the silicon dioxide plane in the intersection part. The second tube in the image starts in the central left part of the picture and passes below the first tube.

The elevated part of the winding is observed in Fig. 1.14, in comparison with Fig.1.13: the brighter parts of the image represent higher segments proving the consistency of the geometry described before. A third and smaller tube is also present in Fig. 1.12b,c and Fig. 1.14. Since this tube is not visible while the sample is tilted as mentioned before, and it looks dark in the AFM height image (see Fig. 1.14), it is possible to conclude that it lays below the junction of the two main tubes and it is not involved in the ribbon. Very high stability of the sample has been observed. SEM and FIB analysis were performed in Berlin while AFM acquisition has been done 6 months later in Salerno. No changes in geometry occurred proving that the adhesion to the SiO₂ surface of the pure MWCNTs was very strong.

1.3 Conclusions

The formation of a photosensitive device due to the local breakdown in an MOS structure with an impurity containing oxide layer has been monitored. A stepwise breakdown of the oxide layer resulted in the formation of a diode like characteristics with further on stable current-voltage characteristics.

Under illumination with white and blue light it was found a high photosensitivity of the resulting structure, probably due to the formation of a local p-n junction due to out-diffusion from the oxide of n-type dopants into the underlying silicon substrate.

Using a blue light LED illumination during the monitoring of the device formation enables the identification of the moment, when a high ratio between photo- and dark current is obtained. After these experiments a good oxide was produced and tested. MWCNTs had been deposited by casting electrophoresis on top of this oxide.

Using three different microscopy techniques: namely AFM, SEM and FIB, the geometry of the interconnection of a single junction between the deposited MWCNTs has been investigated in detail. A very particular twisted interconnection geometry has been observed. Furthermore a strong stability of the sample in time has

been observed proving a strong adhesion of the tubes over the SiO₂ surface.

Chapter 2

Carbon Nanotube Networks

2.1 Technology for pure CNT networks production

2.1.1 Preparation of the solutions

Regarding the nanotube deposition from a solution, one of the most critical steps is the use of an appropriate surfactant [71]. Sodium Dodecyl Sulfate (SDS) is an efficient surfactant for CNTs in water and after the deposition, once CNTs have been fixed by van der Waals forces on the surface of the sample, it can be removed by rinsing with water. Scanning electron microscope (SEM) images of the samples prepared using a SDS containing water solution revealed no evidence of residual SDS after washing.

For the preparation of the solutions SDS was added to milliQ™ water in concentrations of 1% or 10% weight in volume. MWCNTs were added to the solution and the mixture has been sonicated at room temperature for 20min. The used carbon nanotubes were commercially available non-modified type “3100” CNTs from Nanocyl, with a typical length of 0.1-10 μ m and a typical diameter of 10nm. At the end of the sonication process the water results darkened in proportion to the percentage of the SDS. The darkening revealed that the nanotubes clusters were unfastened and they were dispersed uniformly in water. Since some cluster residues were still present in the solution, the solution was centrifuged at 4000rpm for 10min. At the end of the centrifugation process only the supernatant part of the solution was taken.

The solution obtained, as described above, can be considered saturated of MWCNTs and the CNT concentration in the solution depends on the SDS concentration. The absorbance spectra of the solution after sonication and centrifugation for the solution with 10% SDS was also measured. The second solvent used was a mixture

composed of 70% ethanol and 30% dimethyl sulfoxide (DMSO). The MWCNTs were added and the mixture sonicated for 20 min. In this latter case the solution was not centrifuged and it was visible that the MWCNT clusters were not properly unfastened. The solution was diluted in MilliQ™ water in order to obtain a final concentration of 1% in volume.

Differently from the solution, prepared with SDS, the one prepared with ethanol/DMSO in water appeared full of clusters in a transparent medium.

When depositing this solution only the transparent part was taken and this resulted in a MWCNTs network with a very low number of nanotubes.

Sample No.	Solvent/ Surfactant	Medium	Casted Volume	Voltage	Frequency	Time of DEP
1	SDS	MilliQ water	1 μ l	10Vpp AC	15MHz	7min
2	SDS	MilliQ water	1 μ l	10Vpp AC	15MHz	7min
3	Ethanol DMSO	MilliQ water	1 μ l	10Vpp AC	15MHz	7min

Table 2.1. Summary of the procedures for the preparation of the samples shown in this paper. DEP is Di-electrophoresis.

2.1.2 Aluminum gap and substrate

Two aluminum contacts with a gap of 3 μ m were prepared using a lift-off process on top of a thermally oxidized (147 nm thick SiO₂ film) p-type silicon substrate with a resistivity of 20 Ω cm.

The layout of the contact geometry has been shown in Fig. 2.1. The oxide thickness has been measured by spectroscopic ellipsometry and the electrical properties of the SiO₂ layer and of the SiO₂/Si interface as well as the silicon doping concentration have been determined by capacitance spectroscopy measurements.

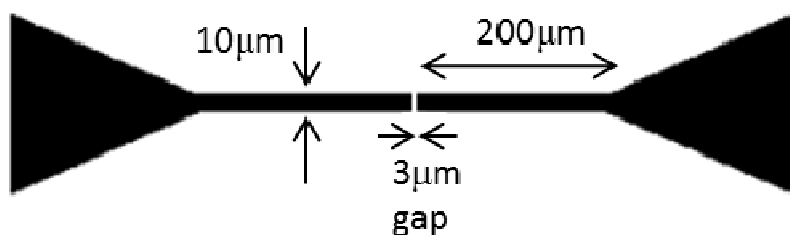


Fig. 2.1 Layout of the aluminum contact structure with a $3\mu\text{m}$ wide gap in the center region.

2.1.3 Casting di-electrophoresis

During the experiments overall 40 depositions were performed. For the preparation of samples 1 and 2 here reported identical procedures were used (see Table 1).

One μL of the SDS solutions was casted on top of the $3\mu\text{m}$ wide micro-gap region and guided the MWCNTs into the gap by a di-electrophoresis process, where a AC sinusoidal electrical signal with an amplitude of 10Vpp and a frequency of 15MHz has been applied for 7 min.

2.1.4 Network morphology

A compaction of the material along the lines of the electric field and in particular at the centre of the micro-gap has been observed (see Fig. 2.2a). A carpet network of MWCNTs is found in the micro-gap (see Fig. 2.2c).

It can be clearly seen that the number of MWCNTs over the contacts is large and that their distribution is quite uniform. It can be also observed that there is no significant presence of MWCNTs outside the region of interest.

When the samples were completely dried after casting they were subsequently rinsed with MilliQ™ water in order to remove the solvent and then dried again.

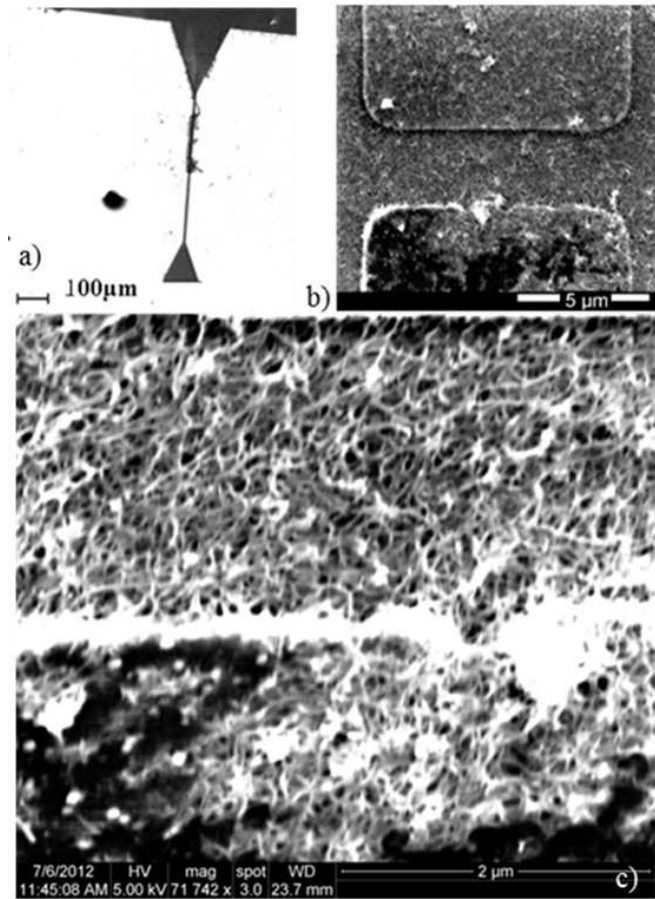


Fig. 2.2. SEM images of sample 1 with a MWCNTs “carpet” in the micro-gap region. The sample has been prepared with CNTs solved with the addition of SDS as surfactant in water. a) MWCNTs inside the aluminum contact gap structure. b) Zoom of the complete gap region. c) Further zoom inside the gap region (aluminum metallization in the lower part of the image).

2.1.5 Characterization equipment

Room temperature electrical characteristics were performed using a Keithley 2400 source measurement unit. The electrophoresis has been performed using a HP 33120A function and arbitrary waveform

generator, applying the AC voltage during the full time of the first drying process.

All the temperature dependent electrical measurements were carried out in a closed-cycle refrigerator system in a wide temperature range between 8K and 325K. The temperature was stabilized using a GaAlAs thermometer and a resistance heater, with the help of a computer controlled PID loop which ensures a temperature stability during the measurements of better than 0.1K. The sample temperature has been measured using a Cernox resistor thermometer in contact with the sample holder. The detailed description of the experimental setup is reported in [72]. Resistance versus temperature $R(T)$ curves have been taken in current-pulsed mode and the voltage drop has been measured with a digital multimeter.

Secondary Electron Microscopy images have been taken using a FEG-SEM (Field Emission Gun-Scanning Electron Microscope) model Inspect F from the FEI Company, based on a thermal field emitter ZrO/W filament (Schottky type) and equipped with a Everhardt-Thornley Secondary Electron Detector (SED). The nominal microscope resolution is 3nm at 1kV in high vacuum ($<6 \times 10^{-4}$ Pa), the acceleration voltage is tunable between 200V and 30kV and the beam current is smaller than 200nA.

2.2 Electrical characterization

2.2.1 Stabilization and noise behavior

The behavior of the devices was investigated right after the formation of the networks by di-electrophoresis. The electrical field has been applied in order to form nanotube networks only within the micro-gap region while the casted drop was drying at room temperature. After drying the residual surfactant in the case of SDS was washed and the sample dried again. After the second drying it has been measured the first current-voltage characteristics. The influence of the washing procedure did not affect the previously formed network. During experiments very high stability of the CNTs has been observed and no changes in geometry occurred, proving that the adhesion of the pure

MWCNTs to the SiO₂ surface was very strong. It has also been tried to move the CNTs by means of an atomic force microscope (AFM) in contact-mode without any modification of the structure. The first 10 current-voltage characteristics show strong electrical instabilities (see Fig. 2.3a and Fig. 2.3b). Each I-V scan was performed from -10V to 10V and back. After these first 10 current-voltage characteristics a current in time measurement was performed, applying a constant voltage of +10V (see Fig. 2.3c). The sampling time was 0.1 sec. During the first 180s the oscillations were faster than the sample rate and the amplitude of the current noise was around 80% of the average current value. Between 180s and about 500s, both frequency and amplitude of the noise slowly decreased. It can be observed the presence of three periods of relative low noise values and discrete current levels interspersed in time segments with higher noise values. After 500s 4 different discrete levels of the sample current can be seen.

After this application of a constant voltage for a certain time, it can be found a stabilization of the characteristics of the sample that started to exhibit a simple resistive behavior without hysteresis (Fig. 2.3d). In the case of samples produced by ethanol/DMSO solvents, resulting in a very low concentration of nanotubes in the gap region (see Fig. 2.4a), it was not possible to observe the former observed stabilization of the current-voltage characteristics and no simple ohmic behavior (see Fig. 2.4b). One of the explanations for this phenomenon can be found in considering that when a big number of CNTs-metal contacts is involved it is more probable that some of them can have large contact area on the metal. In this case the electronic structure calculations, reported in literature, suggest a better electronic coupling between the electrode material and the MWCNTs [73], [74]. In particular Anantram et al. find that the physics of CNTs/metal conduction depended also on the diameter of the CNTs [74], and the latter parameter in our case varies statistically around 10nm. In addition, the random telegraph noise behavior of the current in a CNT field effect transistor has been explained as a random charging and discharging of defects located in the silicon dioxide layer and energetically close to the CNT Fermi level [19].

In our case the presence of aluminum oxide at the interface between aluminum contact and MWCNTs could play the same role at

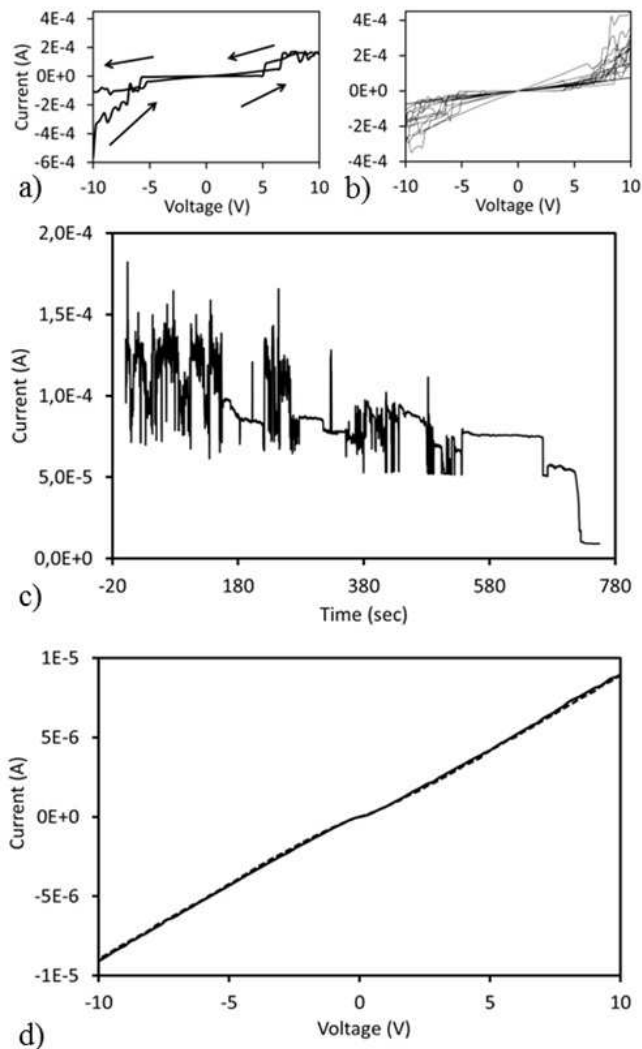


Fig. 2.3. *a) First current-voltage characteristics of sample 2 measured at room temperature (both measurement directions). b) 2nd to 10th room temperature I-V characteristics of sample 2. c) Monitoring of the sample current with a fixed applied voltage of +10V after the termination of the previous 11 current-voltage scans between -10V and 10V d) Current-voltage characteristics (solid line: from negative to positive voltages and dashed line: from positive to negative voltages), measured after the stabilization process with a fixed applied DC voltage of +10V, as monitored in Fig. 2.3c).*

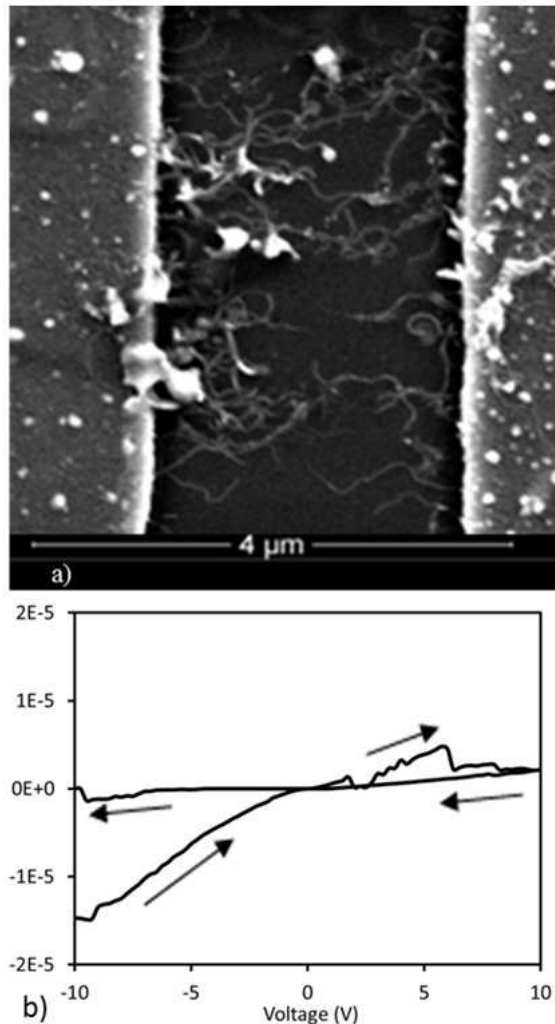


Fig. 2.4. a) Scanning electron microscope image of sample 3 with few nanotubes in the gap region .b) First current-voltage characteristics of sample 3, measured at room temperature (both measurement directions, as indicated by the arrows).

the contact interface. Regarding the stabilization of the electrical characteristics, contacts with very low resistance between an individual single-walled carbon nanotube (SWNT) and palladium (Pd)

electrodes have been obtained using electric-current-induced Joule heating. [75]. The authors deposited SWCNTs onto Pd electrodes pre-patterned on a SiO₂/Si substrate, and achieved the elimination of the tunneling barriers between the SWNTs and the electrodes through annealing [75]. In the case of semiconducting SWNTs, the Schottky barrier is estimated to increase slightly after electrical pulse annealing in some cases, resulting in a relatively high resistance and asymmetrical current-voltage characteristics [75].

This could be a possible explanation for the stabilization of our MWCNT random network, as the application of a constant voltage of 10V can cause local heating and annealing of the nanotube-metal interface.

Since the MWCNTs have not identical electrical properties, for some of them the barrier can be decreased by heating and for others increased. Finally the effect of aluminum contacts on SWCNTs transistors with 300nm contact distance has been explored and compared to those realized with with palladium and titanium contacts [76].

Aluminum contacts resulted in the lowest current (maximum value of about $5 \cdot 10^{-8}$ A) [76]. In our case with a distance of 3 μ m between the aluminum contacts the current is in the μ A-range.

2.2.1 Stable characteristics and temperature behavior

Investigation of sample 1 was performed when a stable behavior was reached. In particular, the temperature behavior of the network has been studied. As clearly evident in Fig. 2.5a and 2.5b, a decreasing resistance with temperature is found in the whole investigated range. This behavior can be interpreted in terms of different theoretical models, used in the case of MWCNTs networks. In particular the most commonly considered are: 1) Luttinger liquid (LL) [77], 2) variable range hopping (VRH) [78], and 3) fluctuation induced tunneling (FIT) [79]. While LL and VRH models completely fail in reproducing the measurements (see the dashed and dotted curves, respectively, in Fig. 2.5b), a qualitative agreement between FIT and the experimental data points is observed (clearly shown by the solid curve of Fig. 2.5b). The lowest reduced χ^2 and the highest coefficient of determination r^2

values, reported in Table 2, support the choice of FIT as the most appropriate theoretical interpretation of the experimental temperature dependence. This is not new and surprising, since similar results have already been shown for HDPE/MWCNTs composites [8, 9]. However, the values of the fitting parameters seem to be significantly different from those found in other carbon nanotubes compounds, probably due

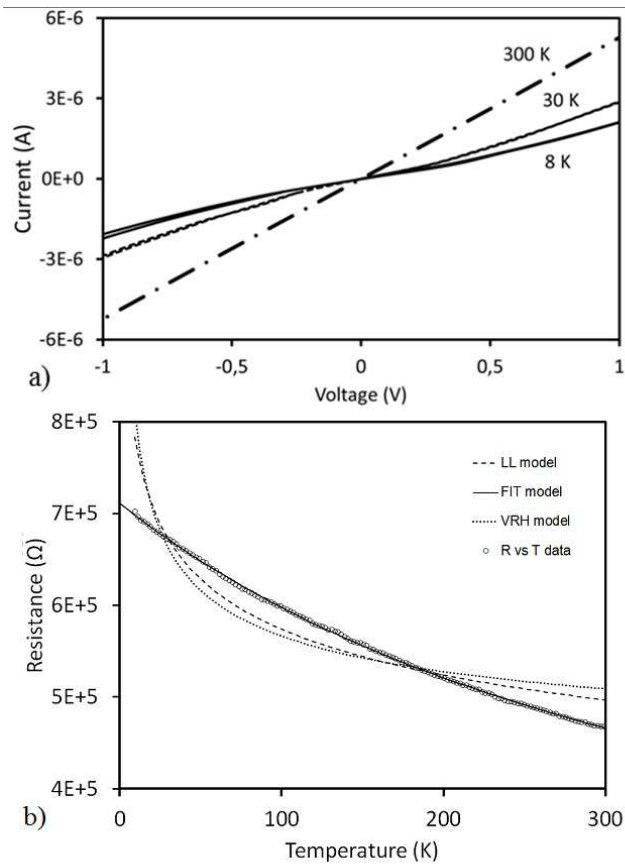


Fig. 2.5. a) Current-voltage characteristics of sample 1 after stabilization, measured at three different temperatures for the structure shown in Fig. 2.2. b) Resistance as a function of temperature of sample 1 after stabilization measured with an applied constant current of $0.5\mu\text{A}$. The curves represent the best fit of the considered theoretical models to the data.

to the possible presence of high-level contact barriers in the system here studied. Although solid interpretation is still missing, the suggestions of previous literature [80], together with the considerations described above, lead us to regard the investigated device as a random resistor network in which the resistors are located at the junctions between carbon nanotubes and the nodes are the conducting pathways connecting different junctions, that is the nanotubes themselves.

<i>Model</i>	χ^2 values	r^2 values
Luttinger liquid	4.45×10^{-2}	0.9006
Variable range hopping	8.23×10^{-1}	0.8163
Fluctuation induced tunneling	1.43×10^{-6}	0.9996

Table 2.2. Reduced χ^2 and coefficient of determination r^2 values, resulting from the fit of the experimental resistance-temperature dependence for the same sample as in Fig. 2.5b).

2.3 Conclusions

In this chapter the techniques used for the construction of temperature sensors based on pure MWCNTs network were reported.

The MWCNTs were deposited from two different solutions leading to different results regarding their morphology: an almost bi-dimensional “carpet” of MWCNTs, and a network composed of a very limited number of MWCNTs. The “carpet” was obtained with a 1% SDS solution in MilliQ water saturated with MWCNTs.

This type of solution described in paragraph 2.1.1 was very stable in time and very reproducible networks could be achieved. For this reason the SDS solution has also be used as starting material for the preparation of the bio-nano-composites, as will be reported in **Chapter 3**.

All the pure nanotube networks were deposited by di-electrophoresis inside an aluminium contact gap with a contact distance of $3\mu\text{m}$.

After the deposition the temperature dependent conductivity of the MWCNTs “carpet” inside the aluminum contact gap has been determined. The temperature behaviour of the conductivity shows a good qualitative agreement with the fluctuation induced tunnelling model for disordered materials.

A rapid reduction of the random telegraph noise present in the virgin devices has been observed after relatively short application of a constant voltage. This increases the possibilities to use aluminum contacts for electronic CNT devices like sensors, where high current levels are not required.

When a different solvent has been used, that resulted in a much lower concentration of CNTs in the micro-gap, a stable electrical behaviour has not been achieved.

Chapter 3

Bio-nano-technology and tissue engineering for electronic and mechanical purposes

In this chapter a new concept is introduced: the possibility to generate new materials useful in a wide range of engineering application from whole biological cells and CNTs. In the first paragraph it has been investigated, if it is possible to use fungal cells to produce temperature sensing elements while in the second paragraph a more general procedure involving for example also isolated cells of tobacco has been explored.

3.1 *Candida albicans*/MWCNTs: a stable conductive bio-nano-composite and its temperature sensing properties.

This paragraph focuses on the first successful production of an artificial tissue produced *in vivo* with whole fungal cells and MWCNTs. As it will be emphasized in *paragraph 3.2* this can be seen as the first prototype of a cyborg tissue. However differently from what is found with the general procedure proposed and achieved in *paragraph 3.2* in this case no “stand alone” material is produced but rather it is applied on top of a SiO₂ layer with gold electrodes like pure CNT networks seen earlier in this thesis. Nevertheless the element can be used as temperature sensor and its performance is better with respect to the pure CNT network devices, especially regarding the stability of the electrical characteristics.

3.1.1 Sample production and morphology

C. albicans yeasts were grown in suspension and agitation at 25°C in RPMI medium and cells, used for this experiment, were collected at

an absorbance of 0.36 OD₆₀₀. Commercially carbon nanotubes (non-modified type “3100” Multi Walled CNTs from Nanocyl™), with a typical length of 0.1-10 μm and a typical diameter of 10 nm were used. The CNTs were dispersed with 1% sodium dodecyl sulfate (SDS) in MilliQ™ water. CNTs were added to the SDS solution and left for 150 min. The CNT suspension was sonicated at room temperature for 20 min, the supernatant was collected and allowed to form a precipitate for 18 hrs. Then the supernatant was collected, centrifuged at 10,000 rpm for 5 min at room temperature and the obtained supernatant was collected again.

The suspension obtained is saturated with CNTs. The final CNT concentration depends on the used SDS concentration. An amount of 750 μl of CNTs were added to 3 ml of *C. albicans* culture with a 20% final concentration of the MWCNT suspension in the growth medium. After incubation at 25°C for additional 24 hrs the artificial “tissue” was collected and deposited onto the coplanar gold electrodes, evaporated on top of the oxidized p-type silicon substrate. The distance between the coplanar contacts was 0.6 mm.

After deposition of the material, the device was dried for 24 hrs at room temperature. For control experiments (RPMI medium with SDS both with and without *C. albicans*) after growth, *C. albicans* alone was centrifuged and the I-V characteristics were measured before drying. However, in this case cells did not form a mechanically stable layer. Instead they formed a layer that in few hours fragmented and pulverized upon drying.

All electrical measurements of *Ca*/MWCNT composites have been performed in a two point-contact geometry using a Keithley model “2400” source measurement unit. Secondary Electron Microscopy images were obtained using a FEG-SEM (Field Emission Gun-Scanning Electron Microscope) model from Inspect F, FEI Co., equipped with a Everhardt-Thornley Secondary Electron Detector (SED).

It was attained a spontaneous aggregation of *C. albicans* when cells were incubated for 24 hours with MWCNTs. The obtained black precipitated viscous material was pipetted out and disposed on a SiO₂ surface.

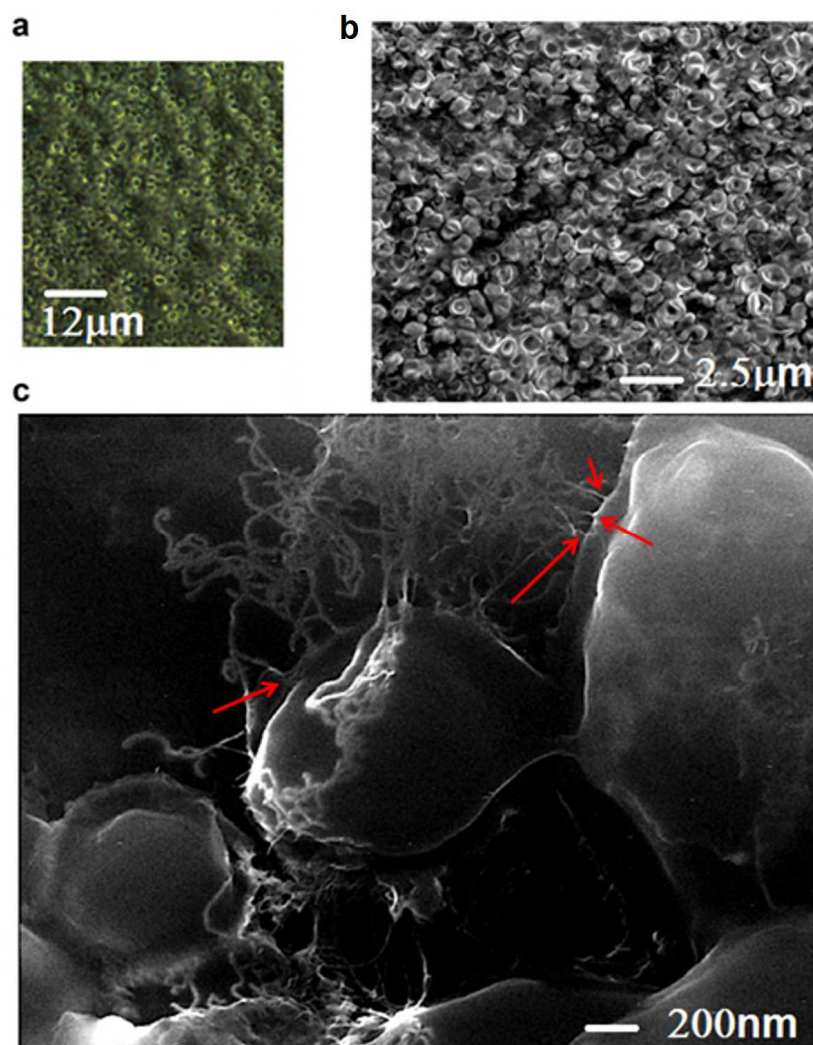


Fig. 3.1 Microscopic images of Ca/MWCNTs composite material (a) Optical microscopy image (magnification 800×) of Ca/MWCNTs material (b) Secondary electron microscopy image of Ca/MWCNTs material (magnification 3,954 ×) (c) Detail of Ca/MWCNTs interaction (SEM image) (magnification 42,739 ×).

When observed by optical microscopy the material resembled an artificial tissue composed of highly packed cells (Fig. 3.1a). In Fig. 3.1b the effect of cell drying is manifested by their “ghost cell” appearance.

A rather specific physical interaction between MWCNTs and *C. albicans* was observed by electron microscopy (Fig. 3.1c) and emphasized by red arrows, suggesting that the cell wall (the most outer part of *Candida* and other yeast cells) may play a major active role in establishing a CNT network and in its stabilization.

3.1.2 Thermo-electrical characterization

The Ca/MWCNTs composite was deposited on top of a silicon substrate covered with a thick thermal SiO₂ layer with coplanar gold electrodes (0.6 mm distant) and the dried samples were subjected to slow temperature cycles in an electronically regulated oven whose temperature was measured using a thin-film thermoelement positioned close to the Ca/MWCNTs composite sample.

All the measurement presented here were performed on a single sample, however, sets of 3 independent experiments (not shown) have been done and each tested material showed similar behavior. Fig. 3.2 shows the monitoring of the oven temperature (blue solid line) and of the resulting sample current (red dashed lines) when applying a constant voltage of 1 V. Due to the low value (about 600 μ W) of the dissipated electrical power in the sample obtained under these conditions, self-heating can be excluded.

The total measurement time was about 12 days. Each cycle, except the first two, was performed with a 12 h period.

The temperature was cycled between a lower value of 25°C and a stepwise increasing upper value, varying from 50° (12 cycles) to 75°C (4 cycles) and finally 100°C (6 cycles). The measured current (see Fig. 3.2) increases monotonically with increasing temperature within every cycle. Furthermore, the room temperature current value after each cooling period strongly increased during the first 12 cycles. The same occurred during steps, coinciding with an increase of the upper cycling temperature (after about 6 days and 8 days).

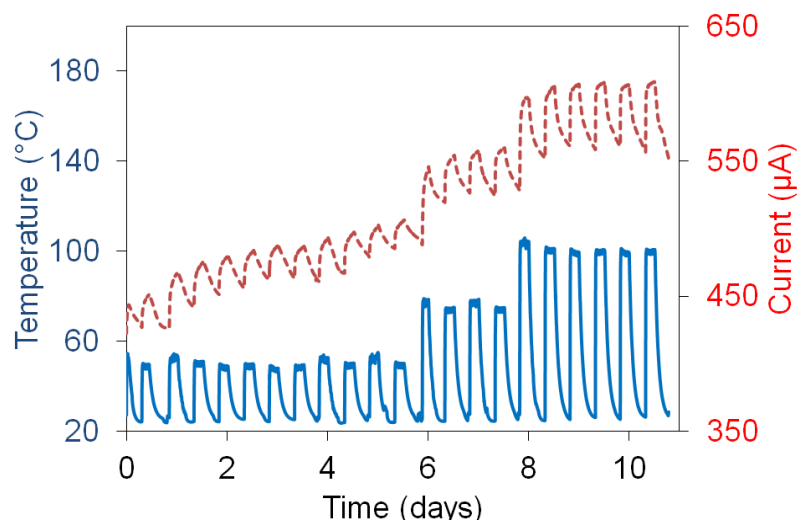


Fig. 3.2 Slow temperature cycling of Ca/MWCNTs composite material. (a) Sample Current (red dashed line) and oven temperature (blue solid line) as a function of time. Tracing of 11 days of temperature cycling is reported. Sampling time: 180 sec.

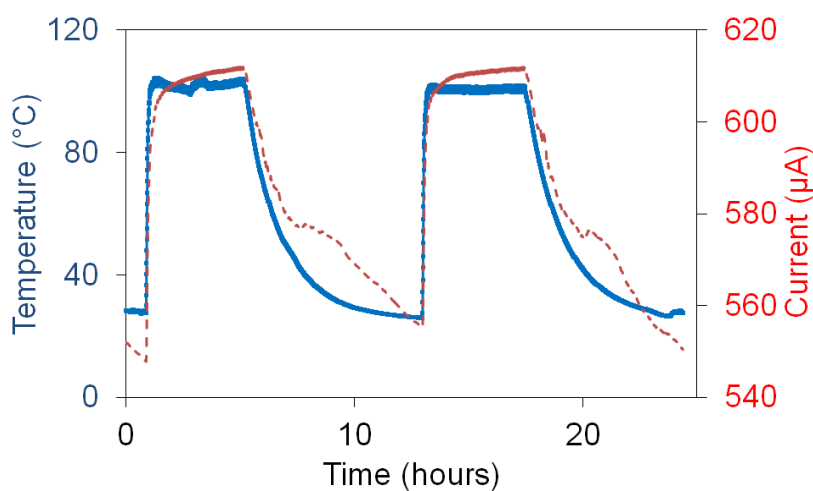


Fig. 3.3. Two additional temperature cycles from 25° to 100°C after stabilization of the sample. Sample current (red dashed line), oven temperature (blue solid line). Sampling time: 15 sec

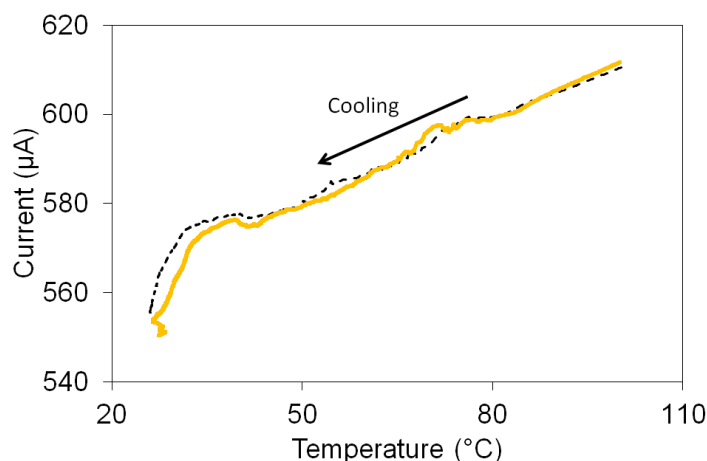


Fig. 3.4. Current vs temperature, for the two cooling cycles reported in Fig. 3.3. Blue dashed line: first cycle, yellow solid line: second cycle.

The increase of the relative room temperature current value was, however, less pronounced during the cycles with an upper temperature of 75°C. An almost stable behavior has been observed during the cycling period with an upper temperature value of 100°C, after the completion of the first cycle. This phenomenon may be due to a release of humidity of the sample or to the rearrangement of CNTs and the *C. albicans* network. After stabilization of the sensing response, a very regular monotonic increase of the sample current with increasing temperature was observed. After 11 days of slow temperature cycling, two additional temperature cycles (1 additional day) with an upper cycling temperature of 100°C were performed with a better time resolution (see Fig. 3.3). A current saturation during the constant high temperature period was observed, but when returning to room temperature the current tended to further decrease. This is also evidenced in Fig. 3.4, in which the sample current is shown as a function of the oven temperature for the two cooling periods only, with sample and oven temperature in equilibrium.

Here it can be observed an almost linear correlation between sample temperature and sample current from 100° to 40°C (slope of +630 nA/°C) and a stronger dependence (about 4 times higher)

between 40° and 25°C. Subsequently, it was measured the current-voltage (I-V) characteristics of the sample at four different temperatures. A perfect linear characteristics has been obtained for all 4 temperatures with a linear regression correlation coefficient R2 equal to 1, as shown for example for the measurement at 25°C in Fig. 3.5. The same figure 3.5 shows control experiments (RPMI medium with SDS both with and without C. albicans), in which no significant electrical conductivity was detected. Fig. 3.6 shows an enlarged area of the I-V characteristics at 4 temperatures and a slightly different slope value. Finally, in Fig. 3.7 temperature dependence of these slope values is shown. A 10% increase of the current value at an applied voltage of 1 V was observed at 100°C, when compared to the value obtained at 25°C. This novel Ca/MWCNTs material, contacted

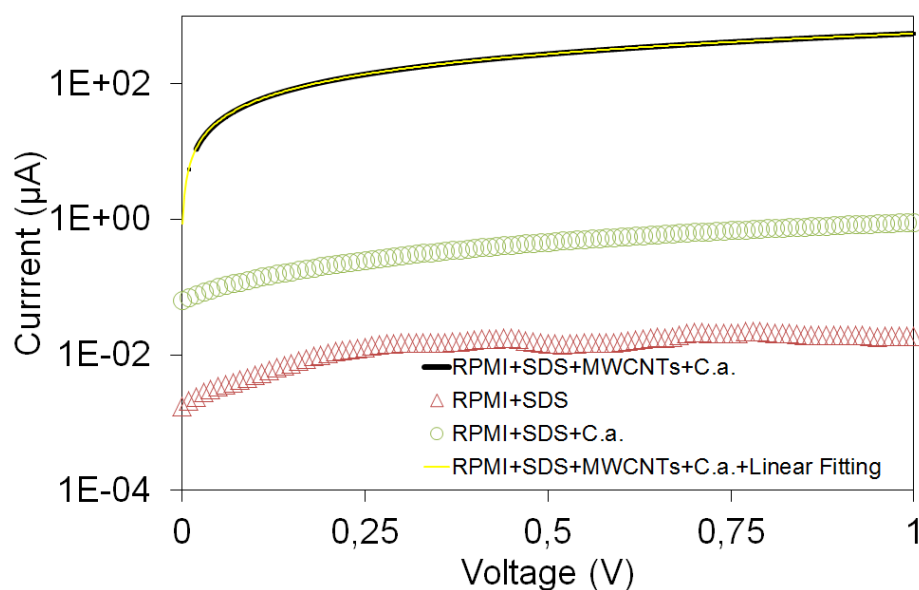


Fig. 3.5 Current-voltage characteristics of Ca/MWCNTs composite material (a) Black dotted line: Current-voltage characteristics at 25°C. Yellow solid line: fit with linear model. Green circles: Current-voltage characteristics of growth medium with solvent and cells. Red triangles: Current-voltage characteristics of growth medium and solvent

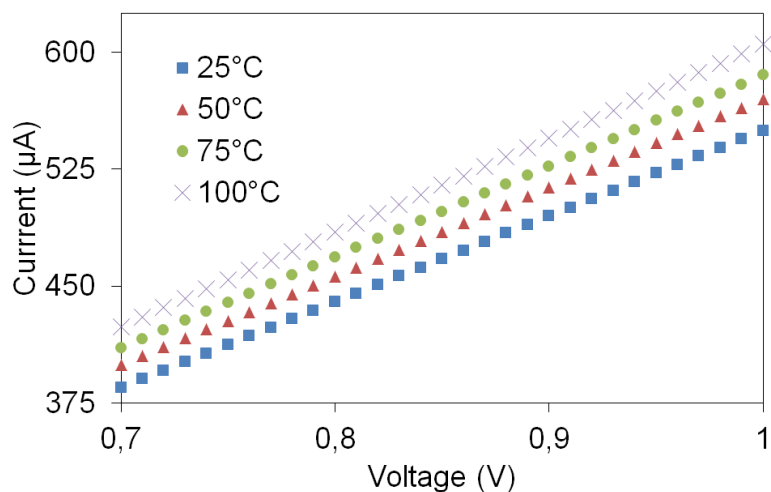


Fig. 3.6 Enlargement of the current-voltage characteristics at different temperatures. Blue squares: 25°C, red triangles: 50°C, green dots 75°C and violet x: 100°C.

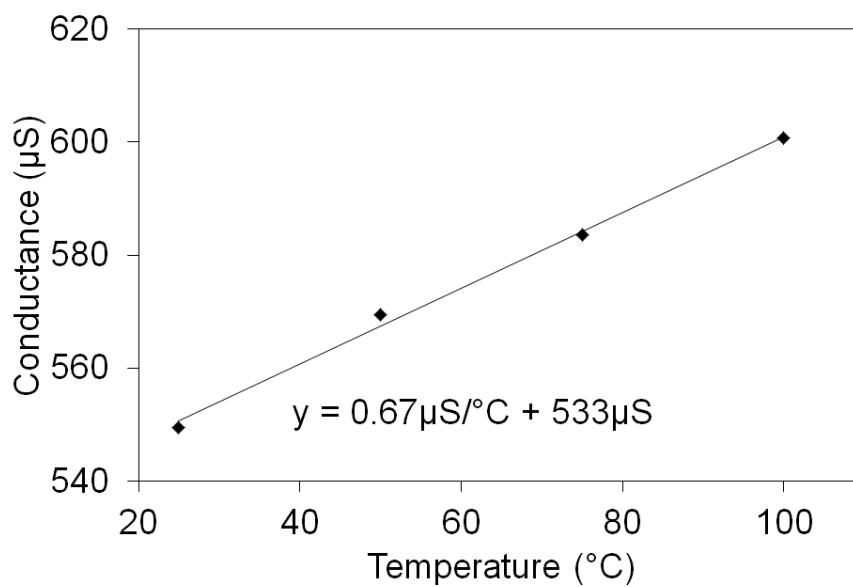


Fig. 3.7 Temperature dependence of the sample conductance.

using gold electrodes has good stability, a perfect linear current-voltage characteristics and, as shown in Fig. 3.5, also a linear dependence of conductance on the ambient temperature after prior heating.

It has been used live *C. albicans* cells to self-structure a Ca/MWCNTs and used it as a temperature-sensing element operative up to 100°C. Microscopy showed that Ca/MWCNTs formed a sort of artificial tissue.

Likewise, dried cells still acted as a stable matrix for the MWCNT network. Good stabilization of the temperature response of the material has been obtained. The artificial tissue also exhibited perfect linear current-voltage characteristics when combined with coplanar gold electrodes.

The produced bio-nano-composite is inexpensive and may be useful in a wide range of electronic applications, ranging from heating to sensing and microwave shielding.

3.2 Cyborg tissues constructed with whole cells and carbon nanotubes: bio-materials for engineering applications

In this paragraph, it is reported, as a proof of concept, that single cells of *C. albicans* and isolated tobacco cells (BY-2), either one in association with multi walled carbon nanotubes (MWCNTs), form artificial tissue materials. MWCNTs allow the formation *in vivo* of a structured gel-like tissue by creating a tight network of tubes that act as artificial “adhesins” [81].

3.2.1 Sample production

Figure 3.8 shows a drawing of the procedure used. The different types of materials produced are: a. BY-2 tobacco cells with 20% of a solution containing 1% SDS (sodium dodecyl sulfate) saturated with

MWCNTs (tobacco/20-MWCNTs); b. *C. albicans* with 6.6% of a solution containing 1% SDS saturated with MWCNTs (Ca/6.6-MWCNTs); c. *C. albicans* with 20% of a solution containing 1% SDS saturated with MWCNTs (Ca/20-MWCNTs).

To obtain a Ca/20-MWCNTs material yeast cells grown at 25°C in RPMI medium (Sigma-Aldrich®, St. Louis, MO) were collected at an absorbance of 0.36 OD₆₀₀ and used for the experiments. To attain a Ca/6.6-MWCNTs yeasts were grown at 25°C in YPD (yeast peptone dextrose) medium. Between 3 and 6 independent cells/MWCNTs suspensions were produced and each analyzed individually.

Commercially available CNTs (non modified type “3100” Multi walled CNTs, Nanocyl™) were used in a solution with SDS as described earlier [82]. Tobacco BY-2 cell line [83] was derived from the callus of seedlings of *Nicotiana tabacum* and propagated in modified Murashige and Skoog medium [84] supplemented with 3% sucrose, 600 µg/ml KH₂PO₄, 0.2 µg/ml 2,4-dichlorophenoxyacetic acid (2,4-D), and 30 µg/ml thiamine-HCl.

Cells were grown in large flasks on a rotary shaker at 130 rpm at 25°C in the dark. Every week 10% of stationary phase cells were transferred to fresh medium.

Spontaneous aggregation of cells was observed with tobacco cells combined with MWCNTs and the obtained material was layered over a plastic film with a plastic policeman rod. Once dried the sample spontaneously detached from the plastic substrate forming a thin film (ca. 142 µm thick). Uniaxial tensile load tests were performed using a displacement-controlled machine (Zwick® BZ 2.5 equipped with a 5N loading cell).

Dual Beam Focused Ion Beam was used to cut the dehydrated *C. albicans* cell by Ga⁺ ions and to obtain SEM pictures. The FIB/SEM instrument was a XL830, DB Magnum FEG, FEI® and Philips®. The FIB part is made by FEI® and mounted on a Philips® SEM. The XL830 series of Scanning Electron Microscopes (SEM) and Focused Ion Beam (FIB) systems contain a large chamber and stage for sample handling.

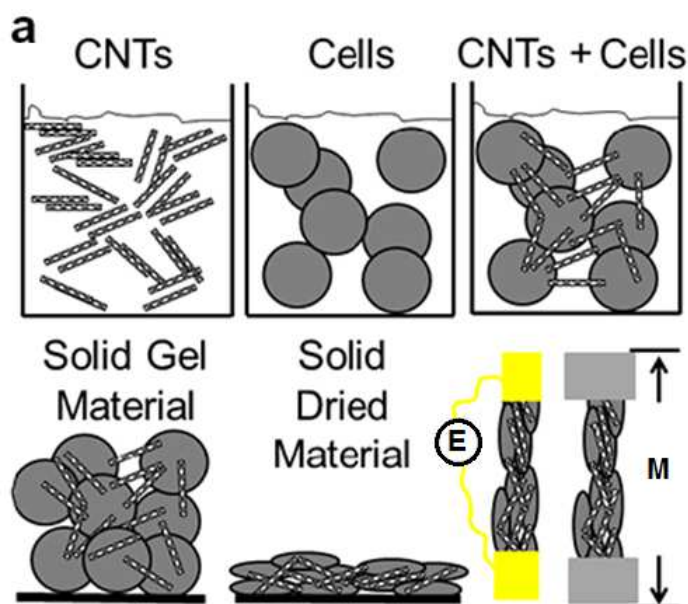


Fig. 3.8 Drawing of the process, used to obtain the materials and the sample geometries for electrical and mechanical characterization.

3.2.2 Material morphology

As seen in microscopic images (Fig. 3.9; 3.10a; 3.11) cells of the composed materials are interconnected by CNTs. After the *in vivo* formation, the materials were dried and the dehydrated cells still acted as a stable matrix for the MWCNT network. When observed by light and scanning electron microscopy (SEM) the material resembled an artificial tissue composed of highly packed cells (Fig. 3.9a,b). In the previous paragraphs it was reported that MWCNTs are inserted into the cell wall of *C. albicans* [82]. Figure 3.9c, Fig. 3.10a and Fig. 3.11 show that MWCNTs surround the cells acting as artificial adhesins. Figure 3.10b shows the effect of cell dehydration as revealed by their “ghost cell” appearance. Using Dual Beam Focused Ion Beam (FIB/SEM) a section of a dried isolated cell without CNTs was cut and it was obtained an image of the treated cell with the incorporated SEM

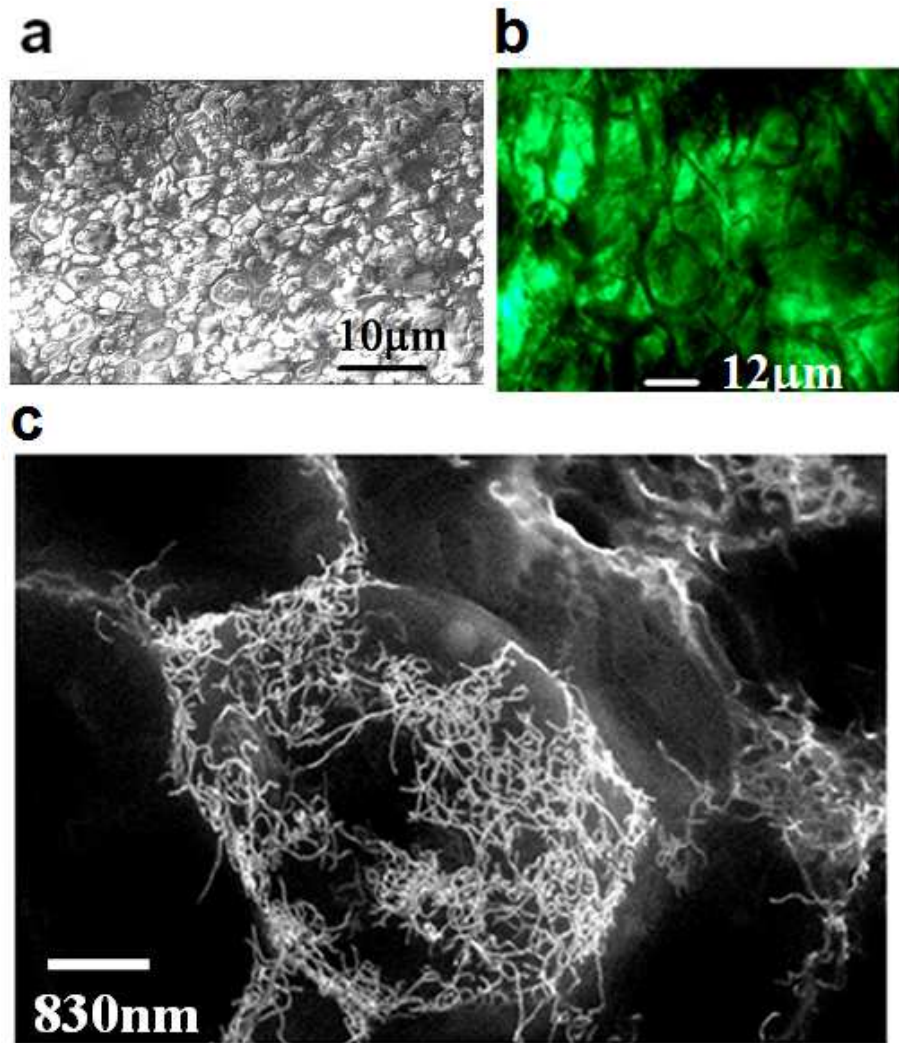


Fig. 3.9 Structure and preparation of cell/MWCNTs cyborg tissues *a.* Microscopy image of dehydrated Ca/20-MWCNTs artificial tissue (SEM image, magnification 2,000×). *b.* Optical microscopy image of dehydrated tobacco/20-MWCNTs artificial tissue (magnification 800x) *c.* Detail of Ca/20-MWCNTs interaction (SEM image) (magnification 12,000×).

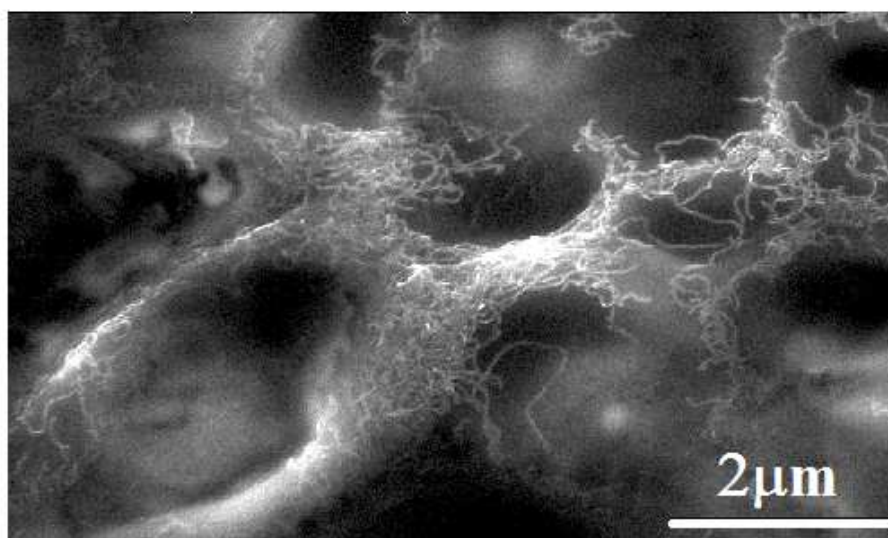
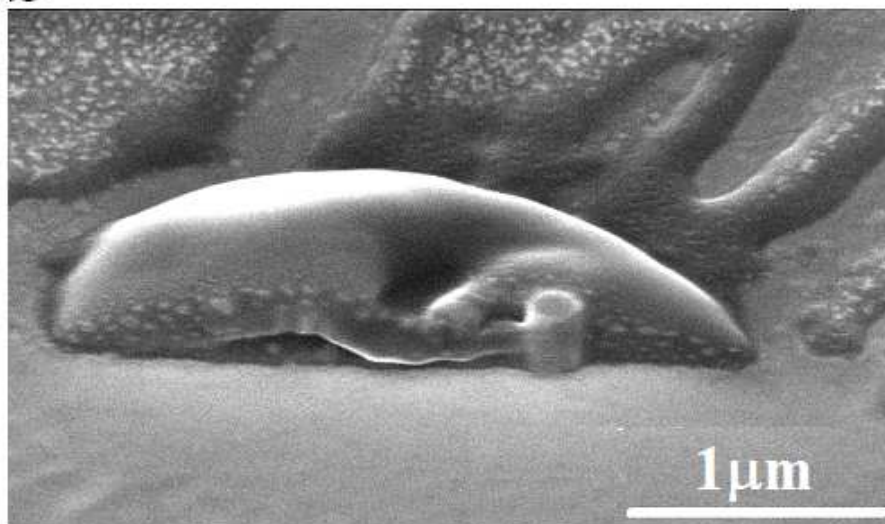
a**b**

Fig. 3.10 *a. SEM image of Ca/20-MWCNTs (magnification 15,000×) with MWCNTs acting as artificial adhesins. b. SEM image of Focused Ion Beam cut section of a dehydrated isolated cell of C.albicans (Magnification 35,000x)*

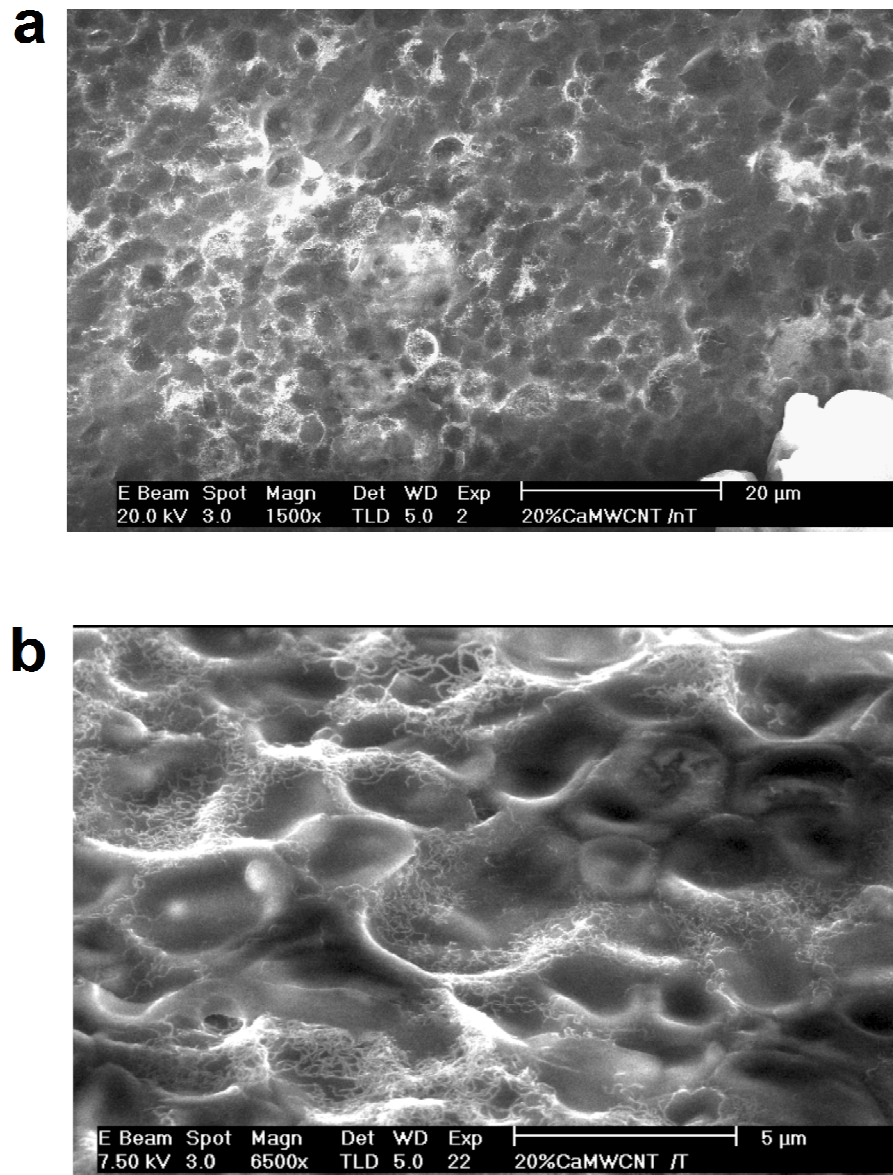


Fig. 3.11 a. SEM image of Ca/20-MWCNTs (magnification 1,500×) b. SEM image of Ca/20-MWCNTs (magnification 6,500×)

3.2.3 Electrical characterization

Figure 3.12 shows the electrical analysis of tobacco/20-MWCNTs material. Co-planar gold electrodes were sputtered on the ends of a material bar (Fig. 3.12b) and the electric field vs. current density characteristics of the material has been measured (Fig. 3.12a).

No hysteresis was detected by changing the applied voltage slope direction. Figure 3.13a reports electrical impedance spectroscopy measurements of the tobacco material at room temperature.

Frequency spanned from 100 Hz to 1 MHz with 2.5 kHz steps. The amplitude of the applied voltage was 50 mV AC and no DC bias voltage was applied. Z' represents the real part of the measured electrical impedance, while Z'' denotes the imaginary part.

The model in Fig. 3.13b is the serial arrangement of two blocks that represent the contribution from the bulk of the material (C_b, R_b) and the effect of the contact interface between gold and the material (R_c, CPE) (see Fig. 3.13c). The Constant Phase Element (CPE) [85] is introduced to model the surface roughness effect on the dielectric behavior [86]. The following equation in the Laplace domain describes the model of Fig. 3.13b.

$$Z(s) = \frac{R_b}{1 + sCR_b} + \frac{R_c}{1 + s^n Q^0 R_c}$$

Where Q^0 is the CPE coefficient and n is the exponent. When $n=1$, the CPE becomes an ideal capacitor. In our case, n is equal, on average, to 0.73 and Q^0 is $8.5 \times 10^{-10} \text{ F} \times \text{s/rad}$.

Biological tissues have been proved to exhibit scale-invariant properties and to be self-similar across multiple physical scales and such properties are described in

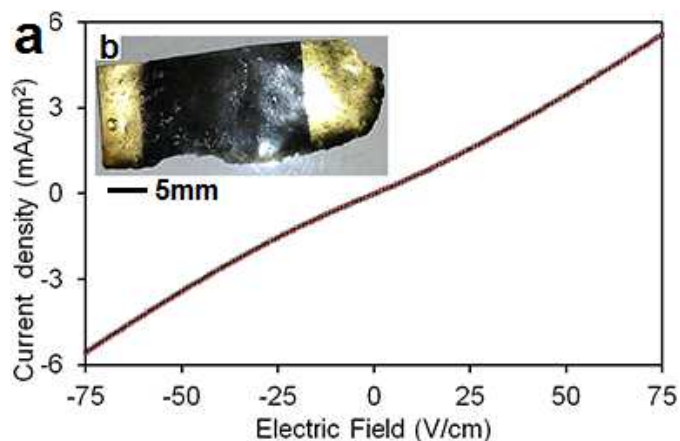


Fig. 3.12 Electrical characteristics of tobacco/20-MWCNTs samples *a.* Electric field vs current density characteristic of the material. *b.* Photograph of the sample with co-planar sputtered gold electrodes.

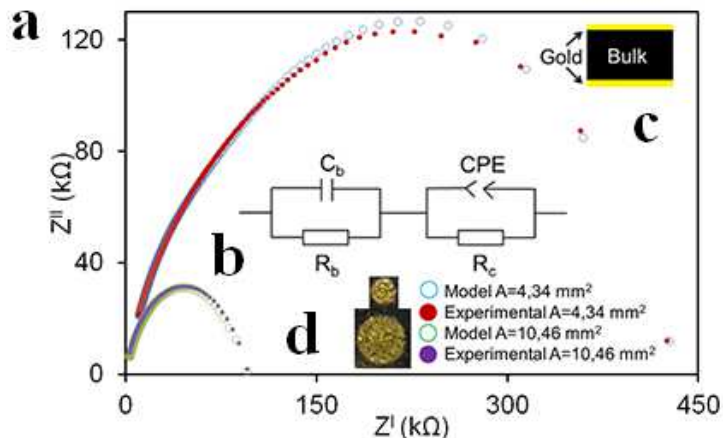


FIG 3.13 *a.* Real part vs imaginary part of the electrical impedance: red dots, impedance spectroscopy relative to larger contacts; blue circles, model simulation; violet dots, impedance spectroscopy relative to smaller contacts; green circles, model simulation. *b.* Schematics of the electrical model of the material. *c.* cross section drawing of the sample sandwiched between gold contacts. *d.* Picture of the top gold contacts (Area=4.34 mm² and Area=10.46 mm²).

the fractal dimension D (Ref. 87). Various models have been proposed to explain CPE with fractal geometry [86].

A model of self-similar fractal electrode [88] gives a relation between the exponent n and the effective fractal dimension D as follows:

$$n = \frac{1}{D - 1}$$

For a rough fractal surface, the fractal dimension D of the surface is between 2 and 3, namely, the surface fills between two and three dimensions [86]. The measurements were performed in sandwich configuration with two different contact areas as shown in Fig. 3.13d and are reported in the legend of Fig. 3.13a. The resulting D has on average a value of 2.4. The obtained value of the relative dielectric constant (ϵ_r) at a frequency of 100 Hz is 390.

Ca/20-MWCNTs composite was deposited on top of a silicon substrate covered with a thick thermal SiO_2 layer with co-planar gold electrodes (0.6 mm apart). Dried samples were subjected to slow temperature cycles in an electronically regulated oven whose temperature was measured using a thin film thermo-element positioned close to the Ca/20-MWCNTs composite sample.

Figure 3.14a shows that the measured current increases monotonically with increasing temperature (steps of 25°C) up to 180°C : a linear thermo electric behavior was detected (Fig. 3.14b). Due to the low value (about $400 \mu\text{W}$) of the dissipated electrical power of the sample obtained under these conditions, self heating can be excluded.

The Ca/20-MWCNTs material contacted with gold electrodes has a good stability and shows a perfect linear current-voltage characteristics (Fig. 3.14c).

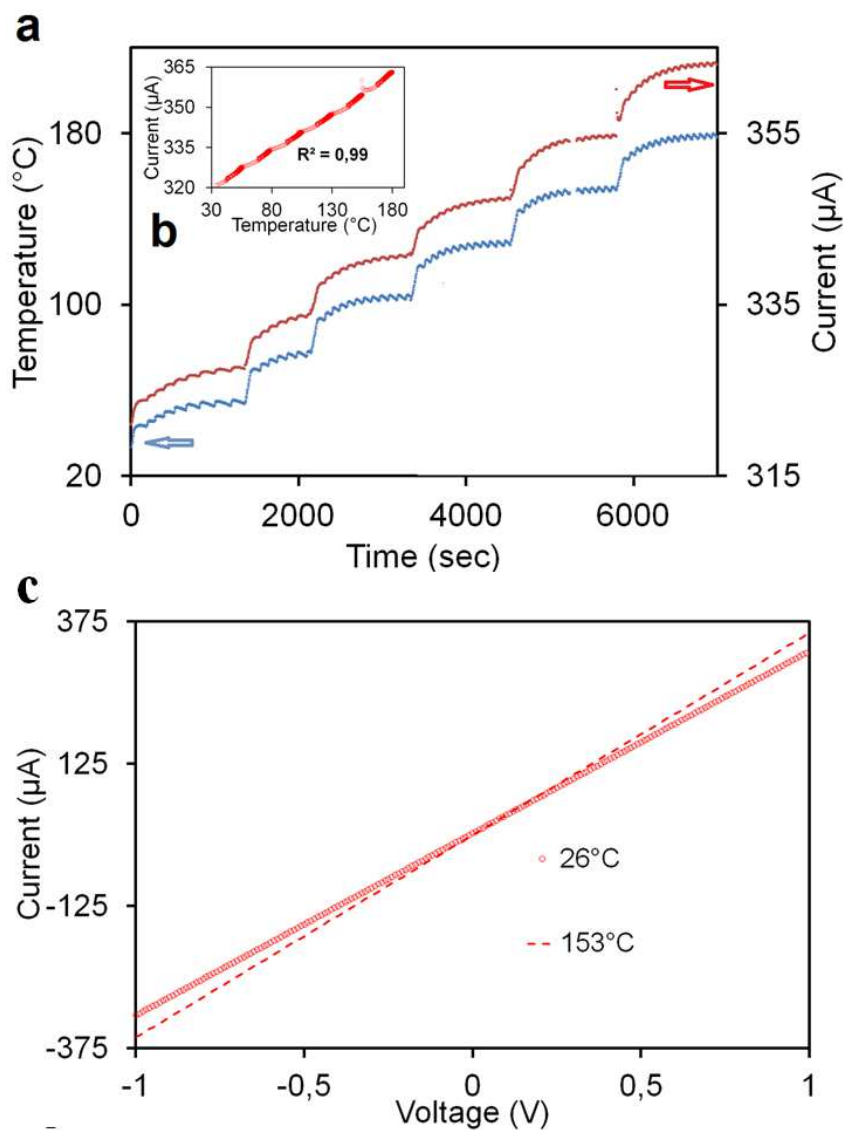


Fig. 3.14 Ca/MWCNTs tissues temperature dependent electrical characteristic. a. Ca/20-MWCNTs: temperature (blue line) and corresponding sample current (red line) vs time measured during a step-stress test up to 180°C. b. Ca/20-MWCNTs: current-temperature characteristics of the sample. c. Ca/20-MWCNTs: current-voltage characteristics at 26° (red circles) and 153°C (dashed line).

3.2.4 Mechanical characterization

Samples of tobacco/20-MWCNTs material with a mass density of 1.03 g/cm^3 (ASTM D792) were cut into long strips (see Fig. 3.16a) and eight sample tractions and five relaxation tests (ASTM D638, ASTM E328) were performed. The behavior was essentially linearly elastic with a mean Young modulus $E = 90.54 \text{ MPa}$ and a mean strength $\sigma^0 = 2.99 \text{ MPa}$.

Values obtained for the Young modulus are similar to that of low density polyethylene [89] while the tensile strength is of the same order of magnitude of the modulus of wood in the fiber direction [90].

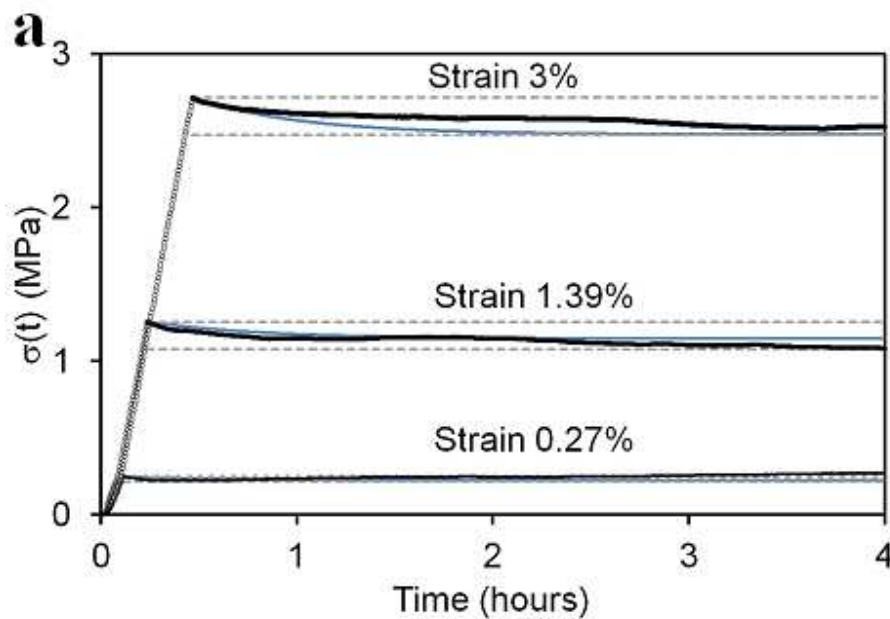


Fig 3.15 Mechanical characteristics of tobacco/20-MWCNTs samples
a. Black lines: relaxation test for three levels of steady strain: 0.27%, 1.39%, 3%. Blue lines: fit with SL model; dashed lines are the initial and the long term levels of stress.

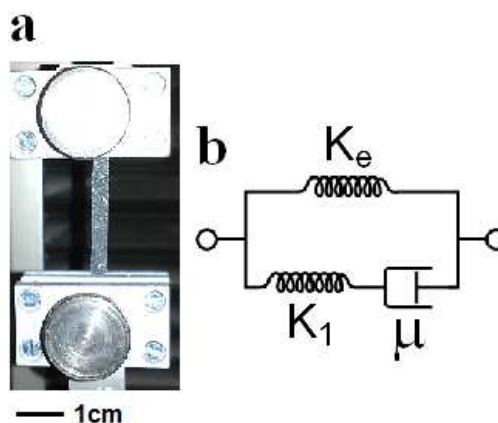


Fig 3.16 a. Photograph of a tobacco/20-MWCNTs bar during mechanical tests. b. SL model schematics with: $K_1 = E - K_e$; $K_e = 82.51$ MPa; $\mu = 16.08$ GPa \times s

Relaxation tests were performed at room temperature to determine the time dependent stress resulting from a steady strain. The material is weakly viscoelastic. Figure 3.15 shows the results of a typical test on a single strip. The parameters modeling the viscoelastic behavior of the material were identified by adopting the Linear-Standard (LS) viscoelastic model shown in Fig. 3.16b, whose relaxation kernel G takes the form:

$$G = K_e + (E - K_e)e^{-\frac{t-t_0}{\tau}}$$

where K_e is the long term rubbery elastic modulus, E the short term glassy modulus, τ is the relaxation time, t_0 is the time at which the relaxation starts and $K_1 = E - K_e$. The best values of the parameters K_e and τ over the five tests performed, determined through nonlinear fit of the data, were: $K_e = 82.51$ MPa, $\tau = 2002$ s, thus $\mu = 16.08$ GPa \times s. Comparison of the predictions of the LS model obtained by setting the parameters to the values given above is shown in Fig. 3.15 (blue lines).

It is important to remark that the measured values of strength and stiffness of tobacco/20-MWCNTs make such material suitable for structural applications.

3.2.5 Optical characterization: a transparent and conductive film

Figure 3.17c shows a photograph of a Ca/6.6-MWCNTs film on an electronic components breadboard, contacted by sputtered gold electrodes at the ends.

Figure 3.17d shows qualitatively the flexibility of the material and, when placed flat, the sample reverted to the original shape. Figure 3.17a shows the spectrum of optical transparency of the sample using a white led as optical source varying from about 30% at 420 nm to about 50% at 720 nm (50 μm). Since both MWCNTs concentration and thickness of the Ca/6.6-MWCNTs are considerably lower than in the case of the Ca/20-MWCNTs sample, previously reported, the conductance is rather small (see Fig. 3.17b). Nevertheless, the behavior of the current voltage characteristics is linear up to 500 V. In summary, a procedure has been established, that explains how to obtain cyborg tissues constructed with whole cells and carbon nanotubes. These bio-materials are appropriate for electric engineering applications since they have performances comparable to existing CNT-composite materials [42,43].

Further, the reported cyborg tissues have values of mechanical strength and stiffness that make such material also suitable for structural applications.

3.3 Conclusions

A *Candida albicans*/multi walled carbon nanotube (Ca/MWCNTs) composite material has been produced. It can be used as a temperature-sensing element operative in a wide temperature range (up to 180 °C). The Ca/MWCNTs composite has excellent linear current-voltage characteristics when combined with coplanar gold

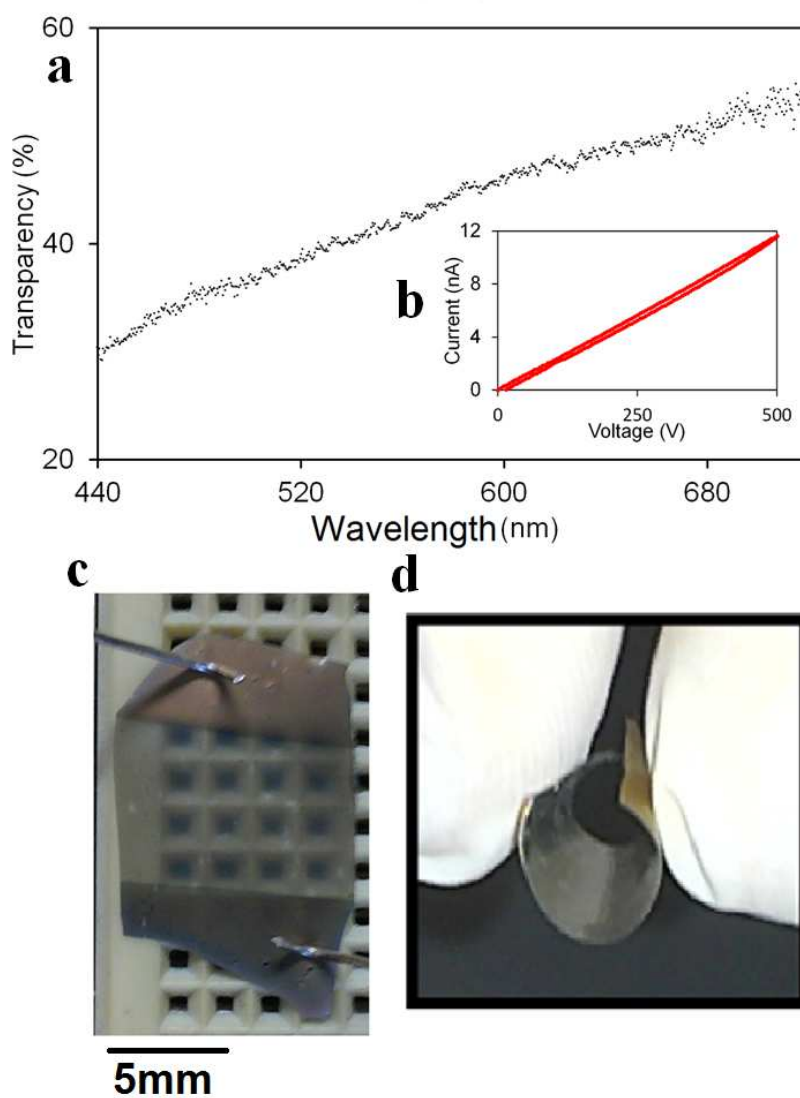


Fig. 3.17 *a. Ca/6.6-MWCNTs: optical transparency spectrum in the visible range. b. Ca/6.6-MWCNTs: current-voltage characteristics up to 500 V. c. Photograph of the Ca/6.6-MWCNTs on an electrical components breadboard. d. Photograph of Ca/6.6-MWCNTs of a thin film bent between two fingers.*

electrodes. Growing cells of *C. albicans* were used to structure the carbon nanotube-based composite. The fungus *C. albicans* combined with MWCNTs co-precipitated as an aggregate of cells and nanotubes that formed a viscous material. Microscopic analyses showed that Ca/MWCNTs formed a sort of artificial tissue. Slow temperature cycling was performed up to 12 days showing a stabilization of the temperature response of the material.

In the present chapter it was also presented a more general procedure in order to obtain the proposed novel artificial materials using, for example, also isolated tobacco cells in combination with different concentrations of carbon nanotubes. The electrical, mechanical, optical, thermo-electrical properties of these materials have been determined. Using tobacco cells it has been obtained a material with low mass density and mechanical properties suitable for structural applications along with high values of the electrical conductivity. It is also reported about theoretical models both for their mechanical and electrical behavior. These findings indicate a procedure for next generation cyborg nano-composite materials.

References

- [1] J. N. Coleman, S. Curran, A. B. Dalton, A. P. Davey, B. McCarthy, W. Blau and R. C. Barklie, "Percolation-dominated conductivity in a conjugated-polymer-carbon-nanotube composite", *Phys Rev B*, Vol. 58, p.R7492, 1998.
- [2] W. Bauhofer and J. Z. Kovacs, "A review and analysis of electrical percolation in carbon nanotube polymer composites", *Compos Sci Technol*, Vol. 69, p.1486, 2008.
- [3] O. Valentino, M. Sarno, N. G. Rainone, M. R. Nobile, P. Ciambelli, H. C. Neitzert and G. P. Simon, "Influence of the polymer structure and nanotube concentration on the conductivity and rheological properties of polyethylene/CNT composites", *Physica E*, Vol. 40, p.2440, 2008.
- [4] F. Deng and Q. S. Zheng, "An analytical model of effective electrical conductivity of carbon nanotube composites", *Appl Phys Lett*, Vol. 92, p.071902, 2008.
- [5] M. Ferrara, H. C. Neitzert, M. Sarno, G. Gorrasi, D. Sannino, V. Vittoria and P. Ciambelli, "Influence of the electrical field applied during thermal cycling on the conductivity of LLDPE/CNTs composites", *Physica E*, Vol. 37, p.66, 2007.
- [6] C. Li, E. T. Thostenson and T. W. Chou, "Dominant role of tunneling resistance in the electrical conductivity of carbon nanotube-based composites", *Appl Phys Lett*, Vol. 91, p.223114, 2007.
- [7] S. Soliveres, J. Gyani, C. Delseny, A. Hoffmann and F. Pascal, " $1/f$ noise and percolation in carbon nanotube random networks", *Appl Phys Lett*, Vol. 90, p.082107, 2007.
- [8] C. Barone, S. Pagano and H.C. Neitzert, "Effect of concentration on low-frequency noise of multi-wall carbon nanotubes in high-density polyethylene matrix", *Appl Phys Lett*, Vol. 97, p.152107, 2010.
- [9] C. Barone, S. Pagano and H.C. Neitzert, "Transport and noise spectroscopy of MWCNT/HDPE composites with different nanotube concentrations" . *J Appl Phys*, Vol. 110, p.113716, 2011.
- [10] C. Barone, D. Imparato, S. Pagano, L. Vertuccio, A. Sorrentino and H.C. Neitzert, "Electrical Noise Characterization of Epoxy/MWCNT Composites", *Lecture Notes in Electrical Engineering*, Vol. 91, p.49, 2010.

- [11] H. C. Neitzert, L. Vertuccio and A. Sorrentino, "Epoxy/MWCNT composite as temperature sensor and electrical heating element", *IEEE Trans Nanotechnol*, Vol. 10, p.688, 2011.
- [12] R. Di Giacomo, H. C. Neitzert, L. Vertuccio, A. Sorrentino and S. Sabbatino, "Application of Epoxy/Carbon Nanotube Composites as Microwave Absorber at Frequencies up to 25 GHz". *Procof of the AISEM 2010 Sensors and Microsystems: Lecture Notes in Electrical Engineering*, Vol. 91, p.455, 2011.
- [13] J. Kim, J.O. Lee, H. Oh, K. H. Yoo and J. J. Kim, "Temperature dependence of the current-voltage characteristics of a carbon-nanotube heterojunction", *Phys Rev B*, Vol. 64, p.161404, 2001.
- [14] Q. Ngo, D. Petranovic, S. Krishnan, A. M. Cassell, Q. Ye, J. Li, M. Meyyappan and C. Y. Yang, "Electron Transport Through Metal-Multiwall Carbon Nanotube Interfaces," *IEEE Trans Nanotechnol*, Vol. 3, p.311, 2004.
- [15] S. Heinze, J. Tersoff, and Ph. Avouris, "Electrostatic engineering of nanotube transistors for improved performance", *Appl Phys Lett*, Vol. 83, p.5038, 2003.
- [16] S. Heinze, J. Tersoff, R. Martel, V. Derycke, J. Appenzeller and Ph. Avouris, "Carbon Nanotubes as Schottky Barrier Transistors", *Phys Rev Lett*, Vol. 89, p.106801, 2002.
- [17] F. Liu, K. L. Wang, D. Zhang, and C. Zhou, "Random telegraph signals and noise behaviors in carbon nanotube transistors", *Appl Phys Lett*, Vol. 89, p. 243101, 2006.
- [18] T. König, G. H. Simon, L. Heinke, L. Lichtenstein and M. Heyde, "Defects in oxide surfaces studied by atomic force and scanning tunneling microscopy", *Beilstein J Nanotechnol*, Vol. 2, p.1, 2011.
- [19] F. Liu, M. Q. Bao, H. J. Kim, K. L. Wang, X. L. Liu, C. Li and C. W. Zhou, "Giant random telegraph signals in the carbon nanotubes as a single defect probe", *Appl Phys Lett*, Vol. 86, p.163102, 2005.
- [20] F. Liu, M. Bao, K. L. Wang, X. Liu, C. Li and C. Zhou, "Determination of the small band gap of carbon nanotubes

- using the ambipolar random telegraph signal”, *Nano Lett*, Vol. 5, p.1333, 2005.
- [21] W. Zhou, L. Ren, F. Lin, L. Jiao, T. Xue, X. Xian and Z. Liu, “An electrical switch based on Ag-tetracyanoquinodimethane sandwiched by crossed carbon nanotube electrodes”, *Appl Phys Lett*, Vol. 93, p.123115, 2008.
- [22] P. G. Collins, M. S. Fuhrer and A. Zettl, “1/f noise in carbon nanotubes”, *Appl Phys Lett*, Vol. 76, p. 894, 2000.
- [23] E. S. Snow, J. P. Novak, M. D. Lay and F. K. Perkins, “1/f noise in single-walled carbon nanotube devices”, *Appl Phys Lett*, Vol. 85, p.4172, 2004.
- [24] R. Cicoria and Y. Sun “Dielectrophoretically trapping semiconductive carbon nanotube networks”, *Nanotechnology*, Vol. 19, p.485303, 2008.
- [25] H. W. Seo, C. S. Han, D. G. C. K. S. Kim b and Y. H. Lee, “Controlled assembly of single SWNTs bundle using Dielectrophoresis”, *Microelectron Eng*, Vol. 81, p.83, 2005.
- [26] Z. B. Zhang, X. J. Liu, E. E. Campbell and S. L. Zhang, “Alternating current dielectrophoresis of carbon nanotubes”, *J Appl Phys*, Vol. 98, p.056103, 2005.
- [27] Christopher M. Welbourn, “P-N-P diamond transistor”, US Patent 5177585, 1991.
- [28] S. J. Tans, A. R. M. Verschueren and C. Dekker, “Room-temperature transistor based on a single carbon nanotube”, *Nature*, Vol. 393, p.49, 1998.
- [29] K. S. Novoselov, A. K. Geim, S. V. Morozov, D. Jiang, Y. Zhang, S. V. Dubonos, I. V. Grigorieva and A. A. Firsov, “Electric Field Effect in Atomically Thin Carbon Films”, *Science*, Vol. 306, p.666, 2004.
- [30] T. Durkop, S. A. Getty, E. Cobas, and M. S. Fuhrer, “Extraordinary Mobility in Semiconducting Carbon Nanotubes”, *Nano Letters*, Vol. 4, p.35, 2004.
- [31] K. I. Bolotin, K. J. Sikes, Z. Jiang, M. Klima, G. Fudenberg, J. Hone, P. Kim, and H. L. Stormer, “Ultrahigh electron mobility in suspended graphene”, *Solid State Comm*, Vol. 146, p.351, 2008.
- [32] E. S. Snow, P. M. Campbell, and M. G. Ancona, ”High-mobility carbon-nanotube thin-film transistors on a polymeric substrate”, *Appl Phys Lett*, Vol. 86, p.033105, 2005.

- [33] S. Li, Z. Yu, S.F. Yen, W. C. Tang, and P. J. Burke, "Carbon Nanotube Transistor Operation at 2.6 GHz", *Nano Lett*, Vol. 4, p.753, 2004.
- [34] D. Wang, Z. Yu, S. McKernan, and P. J. Burke, "Ultrahigh Frequency Carbon Nanotube Transistor Based on a Single Nanotube", *IEEE Trans Nanotechnol*, Vol. 6, p. 400, 2007.
- [35] I. Meric, N. Baklitskaya, P. Kim, and K. L. Shepard, "RF performance of top-gated, zero-bandgap graphene field-effect transistors", *IEEE International Electron Devices Meeting paper no. 4796738*, p.1, 2008.
- [36] Y.M. Li, K. A. Jenkins, A. Valdes-Garcia, J. P. Small, D. B. Farmer and P. Avouris, "Operation of Graphene Transistors at Gigahertz Frequencies", *Nano Lett*, Vol. 9, p. 422, 2009.
- [37] J. Chaste, L. Lechner, P. Morfin, G. Fève, T. Kontos, J. M., Berroir, D. C. Glatli, H. Happy, P. Hakonen and B. Plaçais, "Single Carbon Nanotube Transistor at GHz Frequency", *Nano Lett*, Vol. 8, p.525, 2008.
- [38] Y. M. Lin, C. Dimitrakopoulos, K. A. Jenkins, D. B. Farmer, H.-Y. Chiu, A. Grill and P. Avouris, "100-GHz Transistors from Wafer-Scale Epitaxial Graphene", *Science*, Vol. 327, p.662, 2010.
- [39] J. Vaillancourt, H. Zhang, P. Vasinajindakaw, H. Xia, X. Lu, X. Han, D. C. Janzen, W.S. Shih, C. S. Jones, M. Stroder, M. Y. Chen, H. Subbaraman, R. T. Chen, U. Berger and M. Renn, "All ink-jet-printed carbon nanotube thin-film transistor on a polyimide substrate with an ultrahigh operating frequency of over 5 GHz", *Appl Phys Lett*, Vol. 93, p.243301, 2008.
- [40] A. K. Geim and K. S. Novoselov "The rise of graphene", *Nature Materials*, Vol. 6, p.183, 2007.
- [41] W. Bauhofer and J. Z. Kovacs, "A review and analysis of electrical percolation in carbon nanotube polymer composites", *Compos Sci Technol*, Vol. 69, p.1486, 2009.
- [42] H. C. Neitzert, L. Vertuccio and A. Sorrentino, "A. Epoxy/MWCNT composite as temperature sensor and electrical heating element", *IEEE Trans Nanotechnol*, Vol. 10, p.688, 2011.
- [43] S. P. Bao, G. D. Liang and S. C. Tjong, "Positive temperature coefficient effect of polypropylene/carbon

- nanotube/montmorillonite hybrid nanocomposites”, IEEE Trans Nanotechnol, Vol. 8, p.729, 2009.
- [44] X. L. He, J. H. Du, Z. Ying, H. M. Cheng and X. J. He, “Positive temperature coefficient effect in multiwalled carbon nanotube/high-density polyethylene composites”, Appl Phys Lett, Vol. 86, p.062111, 2005.
- [45] D. Cai, D. Blair, F. J. Dufort, M. R. Gumina, Z. Huang, G. Hong, D. Wagner, D. Canahan, K. Kempa, Z. F. Ren and T. C. Chiles, “Interaction between carbon nanotubes and mammalian cells: characterization by flow cytometry and application”, Nanotechnology, Vol. 19, p.1, 2008.
- [46] K. Kostarelos, L. Lacerda, G. Pastorin, W. Wu, S. Wieckowski, J. Luangsivilay, S. Godefroy, D. Pantarotto, J. P. Briand, S. Muller, M. Prato and A. Bianco, “Cellular uptake of functionalized carbon nanotubes is independent of functional group and cell type”, Nature Nanotechnology, Vol. 2, p.108, 2007.
- [47] X. Yang, Z. Zhou, F. Zheng and Y. Wu, “High sensitivity temperature sensor based on a long, suspended single-walled carbon nanotube array”, Micro Nano Lett, Vol. 5, p.157, 2010.
- [48] M. Imai, K. Akiyama, T. Tanaka and E. Sano, “Highly strong and conductive carbon nanotube/cellulose composite paper”, Compos Sci Technol, Vol. 70, p.1564, 2010.
- [49] P. Lu and Y. L. Hsieh, “Multiwalled carbon nanotube (MWCNT) reinforced cellulose fibers by electrospinning”, ACS Appl Mater Interfaces, Vol. 2, p.2413, 2010.
- [50] C. L. Phillips, C. S. Yah, S. E. Iyuke, K. Rumbold and V. Pillay, “The cellular response of *Saccharomyces cerevisiae* to multi-walled carbon nanotubes (MWCNTs)”, J Saudi Chem Soc, doi:10.1016/j.jscs.2012.01.005
- [51] A. Bianco, K. Kostarelos and M. Prato, “Applications of carbon nanotubes in drug delivery”, Curr Opin Chem Biol, Vol. 9, p.674, 2005.
- [52] L. Gao, L. Nie, T. Wang, Y. Qin, Z. Guo, D. Yang and X. Yan, “Carbon Nanotube Delivery of the GFP Gene into Mammalian Cells”, Chembiochem, Vol. 7, p.239, 2006.
- [53] K. T. Al-Jamal, “Cellular uptake mechanisms of functionalised multi-walled carbon nanotubes by 3D electron tomography imaging”, Nanoscale, Vol. 3, p.2627, 2011.

- [54] M. Tuzena, K. O. Saygia, C. Ustab and M. Soylakc, "Pseudomonas aeruginosa immobilized multiwalled carbon nanotubes as biosorbent for heavy metal ions", *Bioresour. Technol*, Vol. 99, p.1563, 2008.
- [55] R. Di Giacomo, C. Barone, S. Pagano, P. Sabatino, G. Carapella, R. Adami, C. Boit and H. C. Neitzert, "Stabilization of the electrical characteristics of Carbon Nanotubes Networks in an aluminum contact micro-gap", private communication
- [56] B. Tian, J. Liu, T. Dvir, L. Jin, J. H. Tsui, Q. Qing, Z. Suo, R. Langer, D. S. Kohane and C. M. Lieber. "Macroporous nanowire nanoelectronic scaffolds for synthetic tissues", *Nature Materials*, Vol. 11, p.986, 2012.
- [57] G. D. Nicodemus and S. J. Bryant, "Cell Encapsulation in Biodegradable Hydrogels for Tissue Engineering Applications", *Tissue Engineering Part B Rev*, Vol. 14, p.149, 2008.
- [58] J. S. Katz and J. A. Burdick, "Hydrogel mediated delivery of trophic factors for neural repair", *Wiley Interdiscip Rev Nanomed Nanobiotechnol*, Vol. 1, p.128, 2009.
- [59] M. C. Cushing and K. S. Anseth, "Hydrogel Cell Cultures", *Science*, Vol. 316, p.1133, 2007.
- [60] W. Lee and J. Park, "The design of a heterocellular 3D architecture and its application to monitoring the behavior of cancer cells in response to the spatial distribution of endothelial cells", *Adv Mater*, Vol. 24, p.5339, 2012.
- [61] J. B. Lee, S. Peng, D. Yang, Y. H. Roh, H. Funabashi, N. Park, E. J. Rice, L. Chen, R. Long, M. Wu and D. Luo, "A mechanical metamaterial made from a DNA hydrogel", *Nature Nanotechnology*, Vol. 7, p.816, 2012.
- [62] C. J. Bettinger and Z. Bao. "Biomaterials-based organic electronic devices", *Polym Int*, Vol. 59, p.563, 2010.
- [63] S. Ashok, P. P. Sharma and S. J. Fonash, "Spray-deposited ITO-Silicon SIS heterojunction solar cells", *IEEE Trans Electron Dev*, Vol. 27, p.725, 2005.
- [64] H. C. Neitzert, "Characterization of electronic transport in amorphous silicon / crystalline silicon photodiodes", *SPIE Proc* 1985, p.530, 1993.

- [65] T. Kinoshita, D. Fujishima, A. Yano, A. Ogane, S. Tohoda, K. Matsuyama, Y. Nakamura, N. Tokuoka, H. Kanno, H. Sakata, M. Taguchi and E. Maruyama, "The approaches for high efficiency HITTM solar cell with very thin (< 100 μm) silicon wafer over 23%", Proc of the 26th PVSEC, p.871, 2011.
- [66] H. C. Neitzert, S. Schwertheim, K. Meusinger, M. Leinhos and W. R. Fahrner, "Heterojunction solar cell fabricated by spin-coating of a CNT/PEDOT:PSS heteroemitter on top of a crystalline silicon absorber", SPIE Proc, 7364, p.73460L-1, 2009.
- [67] A. V. Petrov, D. Fink, G. Richter, P. Szimkowiak, A. Chemseddine, P. S. Alegaonkar, A. S. Berdinsky, L. T. Chadderton and W. R. Fahrner, "Creation of nanoscale electronic devices by the swift heavy ion technology", Proc of the 4th Siberian Russian Workshop on Electron. Devices and Materials, p.40, 2003.
- [68] H. C. Neitzert, A. Piccirillo and B. Gobbi, "Sensitivity of proton implanted VCSELs to electrostatic discharge pulses", IEEE J of Selected Topics in Quantum Electronics, Vol. 7, p.231, 2001.
- [69] H. C. Neitzert, "ESD sensitivity of AlGaAs and InGaAsP based Fabry-Perot laser diodes", Microelectron. Reliab, Vol. 50, p.1563, 2010.
- [70] H. C. Neitzert, "Optical gain at low bias voltages in electrostatic-discharge-damaged silicon p-i-n photodiodes", Phil Mag B, Vol. 80, p.799, 2000.
- [71] L. Vaisman, H. D. Wagner and G. Marom, "The role of surfactants in dispersion of carbon nanotubes", Adv Colloid Interface Sci, Vol. 128, p.37, 2007.
- [72] C. Barone, A. Galdi, S. Pagano, O. Quaranta, L. Méchin, J.-M. Routoure and P. Perna, "Apparent volume dependence of 1/f noise in thin film structures: Role of contacts", Rev Sci Instrum, Vol. 79, p.053908, 2008.
- [73] M. P. Anantram, "Which nanowire couples better electrically to a metal contact: Armchair or zigzag nanotube?", Appl Phys Lett, Vol. 78, p.2055, 2001.
- [74] M. P. Anantram, S. Datta and Y. Xue, "Coupling of carbon nanotubes to metallic contacts", Phys Rev B Condens Matter, Vol. 61, p.14 219, 2000.

- [75] Y. Woo, G. S. Duesberg and S. Roth. “Reduced contact resistance between an individual single-walled carbon nanotube and a metal electrode by a local point annealing”, *Nanotechnology*, Vol. 18, p.095203, 2007.
- [76] Z. Chen, J. Appenzeller, J. Knoch, Y.-m. Lin and P. Avouris “The role of metal–nanotube contact in the performance of carbon nanotube field-effect transistors“, *Nano Letters*, Vol. 5, p.1497, 2005.
- [77] M. Bockrath, D.H. Cobden, J. Lu, A.G. Rinzler, R.E. Smalley, L. Balents and P.L. McEuen, “Luttinger-liquid behaviour in carbon nanotubes”, *Nature*, Vol. 397, p.598, 1999.
- [78] Nevill Francis Mott and E. A. Davis, “Electronic processes in non-crystalline materials”, Oxford, Eng Clarendon Press, 1979.
- [79] P. Sheng, “Fluctuation-induced tunneling conduction in disordered materials”, *Phys Rev B*, Vol. 21, p.2180, 1980.
- [80] E. S. Snow, J. P. Novak, P. M. Campbell and D. Park, “Random networks of carbon nanotubes as an electronic material”, *Appl Phys Lett*, Vol. 82, p.2145, 2003.
- [81] C. J. Nobile, J. E. Nett, D. R. Andes and A. P. Mitchell. “Function of *Candida albicans* Adhesin Hwp1 in Biofilm Formation”, *Eukaryot Cell*, Vol. 5, p.1604, 2006
- [82] R. Di Giacomo, B. Maresca, A. Porta, P. Sabatino, G. Carapella and H. C. Neitzert, “*Candida albicans*/MWCNTs: a stable conductive bio-nanocomposite and its temperature sensing properties”. *IEEE Trans Nanotechnol*, doi:10.1109/TNANO.2013.2239308
- [83] T. Nagata, Y. Nemoto and S. Hasezawa, “Tobacco BY-2 cell line as the "HeLa" cell in the cell biology of higher plants”, *Int Rev Cytol*, Vol.132, p.1, 1992.
- [84] T. Murashige and F. Skoog, “A revised medium for a rapid growth and bioassay with tobacco tissue cultures”, *Physiol Plant*, Vol. 15, p.473, 1962.
- [85] K.S. Cole, “Electric impedance of suspensions of spheres”, *J Gen. Physiol.* Vol. 36, p.12, 1928.
- [86] J. Zhang, M. Mine, D. Zhu and M. Matsuo. “Electrical and dielectric behaviors and their origins in the three-dimensional

- polyvinyl alcohol/MWCNT composites with low percolation threshold”, *Carbon*, Vol. 47, p.1311, 2009.
- [87] X. Wang, F. F. Becker and P. R. C. Gascoyn. “The fractal dimension of cell membrane correlates with its capacitance: A new fractal single-shell model”, *Chaos*, Vol. 20, p.043133, 2010.
- [88] L. Nyikos and T. Pajkossy, “Fractal dimension and fractional power frequency dependent impedance of blocking electrodes”. *Electrochim. Acta*, Vol. 30, p.1533, 1985.
- [89] S. Rostami, “Polymer Blends: Structure and Properties”, *Encyclopedia of Materials: Science and Technology* 7202, 2001.
- [90] ASTM. Standard methods for testing small clear specimens of timber. ASTM D143-94. West Conshohocken, PA: American Society for Testing and Materials.

Acknowledgments

I thank very much for their precious contribution:

H.C. Neitzert

Dept. Industrial Engineering
University of Salerno, Italy.
Supervising.

A. Leone, C. Vaccaro, A. Porta, N. Armenante

Dept. of Pharmacy, Div. of Bio Medicine,
University of Salerno, Italy.
Cell culture.

P. Sabatino, G. Carapella.

"E. R. Caianiello", and CNR SPIN
University of Salerno, Italy
Preparation of gold contacts, SEM microscopy.

S.Pagano, C.Barone

"E. R. Caianiello", and CNR SPIN
University of Salerno, Italy
Termo-electrical measurements on pure CNN.

H. Wegner , C. Boit , U.Kerst

Institute of High Frequency and Semiconductor System
Technologies, Section Semiconductor Devices
TU Berlin, Germany
Aluminum microgaps preparation, SEM microscopy and
FIB, gold sputtering.

M. Angelillo

Dip. Civil Engineering

Experimental and theoretical biomechanics.

G. Landi,

Faculty of Mathematics and Computer Science,

Fern Universität, Hagen,

Electrical modeling.

V. Speranza

Dept. Industrial Engineering

University of Salerno, Italy

AFM microscopy.

R. Adami

Dept. Industrial Engineering

University of Salerno, Italy

SEM microscopy, gold sputtering.

A. De Girolamo, R. Diana

ENEA Research Center,

Portici (NA), Italy.

CNT solutions, SEM microscopy.

I want to thank very much **Bruno Maresca** for teaching me the difference between science and stamp collection. More than half of the ideas reported in the present thesis are the fruits of everyday conversations in his office. I am sure that without him I would have abandoned science long ago before beginning.